ResearchGate

See discussions, stats, and author profiles for this publication at: https://www.researchgate.net/publication/357865860

Non-coding small nucleolar RNA SNORD17 promotes the progression of hepatocellular carcinoma through a positive feedback loop upon p53 inactivation

Article *in* Cell Death and Differentiation · January 2022

DOI: 10.1038/s41418-022-00929-w

CITATIONS
13

READS
43

15 authors, including:

Jingyu Liao
Huazhong University of Science and Technology
11 PUBLICATIONS **126** CITATIONS
SEE PROFILE

Huang Zhao
Huazhong University of Science and Technology
19 PUBLICATIONS **346** CITATIONS
SEE PROFILE

Some of the authors of this publication are also working on these related projects:

BONE METASTASIS View project

All content following this page was uploaded by Huang Zhao on 03 April 2023.

The user has requested enhancement of the downloaded file.

CDDpress

www.nature.com/cdd

ARTICLE

Check for updates

Non-coding small nucleolar RNA SNORD17 promotes the progression of hepatocellular carcinoma through a positive feedback loop upon p53 inactivation

Junnan Liang[1,2,3,6], Ganxun Li[1,2,3,6], Jingyu Liao[1,2,3,6], Zhao Huang[1,2,3,6], Jingyuan Wen[1,2,3], Yu Wang[1,2,3], Zeyu Chen[1,2,3], Guangzhen Cai[1,2,3], Weiqi Xu[1,2,3], Zeyang Ding[1,2,3], Huifang Liang[1,2,3], Pran K. Datta[4], Liang Chu[1,2,3]✉, Xiaoping Chen[1,2,3,5]✉ and Bixiang Zhang[1,2,3,5]✉

© The Author(s), under exclusive licence to ADMC Associazione Differenziamento e Morte Cellulare 2022

Recent evidence suggests that small nucleolar RNAs (snoRNAs) are involved in the progression of various cancers, but their precise roles in hepatocellular carcinoma (HCC) remain largely unclear. Here, we report that SNORD17 promotes the progression of HCC through a positive feedback loop with p53. HCC-related microarray datasets from the Gene Expression Omnibus (GEO) database and clinical HCC samples were used to identify clinically relevant snoRNAs in HCC. SNORD17 was found upregulated in HCC tissues compared with normal liver tissues, and the higher expression of SNORD17 predicted poor outcomes in patients with HCC, especially in those with wild-type p53. SNORD17 promoted the growth and tumorigenicity of HCC cells in vitro and in vivo by inhibiting p53-mediated cell cycle arrest and apoptosis. Mechanistically, SNORD17 anchored nucleophosmin 1 (NPM1) and MYB binding protein 1a (MYBBP1A) in the nucleolus by binding them simultaneously. Loss of SNORD17 promoted the translocation of NPM1 and MYBBP1A into the nucleoplasm, leading to NPM1/MDM2-mediated stability and MYBBP1A/p300-mediated activation of p53. Interestingly, p300-mediated acetylation of p53 inhibited SNORD17 expression by binding to the promoter of SNORD17 in turn, forming a positive feedback loop between SNORD17 and p53. Administration of SNORD17 antisense oligonucleotides (ASOs) significantly suppressed the growth of xenograft tumors in mice. In summary, this study suggests that SNORD17 drives cancer progression by constitutively inhibiting p53 signaling in HCC and may represent a potential therapeutic target for HCC.

Cell Death & Differentiation; https://doi.org/10.1038/s41418-022-00929-w

INTRODUCTION

Hepatocellular carcinoma (HCC) is one of the most prevalent and lethal human malignancies worldwide [1, 2]. Although HCC treatment has dramatically improved over the last decades, the incidence and cancer-specific mortality of HCC continues to increase in many countries, mainly due to the limited understanding of the underlying molecular pathogenesis and limited available therapies for HCC [3, 4]. Thus, more researches are needed to obtain a deeper understanding of pathological processes driving the progression of HCC.

Small nucleolar RNAs (snoRNAs) are conserved noncoding RNAs with a length of 60 to 300 nucleotides. They are well-known for their role as small nucleolar ribonucleoproteins (snoRNPs) guides in post-transcriptional modification and maturation of ribosomal RNAs (rRNAs) [5]. Accordingly, snoRNAs were recognized for playing housekeeping functions due to their critical roles in rRNA maturation [6, 7]. Despite that, other functions of snoRNAs remain largely unknown. Nevertheless, evidence showed that snoRNAs are involved in oncogenesis and can act as prognostic markers in various cancers [8–12]. Cui et al. reported SNORA23 was upregulated in human pancreatic ductal adenocarcinoma (PDAC) and promoted PDAC cell proliferation and invasion through increasing expression of SYNE2 [8]. In HCC, Wang et al. reported that integrating a promoter-enhancer into the mouse Rian gene through in vivo gene targeting with adeno-associated viruses could initiate HCC. The snoRNAs encoded in Rain were upregulated in tumor tissues, which suggested the upregulation of snoRNAs could play an oncogenic role in HCC [13]. Xu et al. found that SNORD113-1 suppressed HCC tumorigenesis by inactivating the phosphorylation of ERK1/2 and SMAD2/3 in MAPK/ERK and TGF-β pathways respectively [14]. These studies imply the critical roles of snoRNA in HCC formation and progression. SNORD17, a C/D box snoRNA, was firstly identified in mouse and known as guide for the 2′-O-ribose methylation for

[1]Hepatic Surgery Center, Tongji Hospital, Tongji Medical College, Huazhong University of Science and Technology, Wuhan, China. [2]Clinical Medical Research Center of Hepatic Surgery at Hubei Province, Wuhan, China. [3]Hubei Key Laboratory of Hepato-Pancreatic-Biliary Diseases, Tongji Hospital, Tongji Medical College, Huazhong University of Science and Technology, Wuhan, China. [4]Division of Hematology and Oncology, Department of Medicine, UAB Comprehensive Cancer Center, Birmingham, AL, USA. [5]Key Laboratory of Organ Transplantation, Ministry of Education; NHC Key Laboratory of Organ Transplantation; Key Laboratory of Organ Transplantation, Chinese Academy of Medical Sciences, Wuhan, China. [6]These authors contributed equally: Junnan Liang, Ganxun Li, Jingyu Liao, Zhao Huang. ✉email: Liangchu@tjh.tjmu.edu.cn; chenxpchenxp@163.com; bixiangzhang@163.com

Edited by C. Borner

Received: 7 July 2021 Revised: 13 December 2021 Accepted: 23 December 2021
Published online: 15 January 2022

rRNA [15]. However, whether and how SNORD17 is involved in HCC processes remain unclear.

The tumor suppressor p53 acts as a potent transcription factor. It can be activated in response to DNA damage or the aberrant activation of oncogenes leading to induction of a wide variety of cellular processes including cell cycle arrest, apoptosis and senescence [16, 17]. p53 is frequently inactivated by mutations or deletions in cancers, including HCC. Moreover, studies have demonstrated that post-translational modifications of p53, such as ubiquitination, phosphorylation, and acetylation, are also involved in the inactivation of p53 that have crucial role in HCC progression [18, 19]. Many noncoding RNAs were found to play critical roles in the p53 signaling network, including miRNA and lncRNA [20]. Nevertheless, the precise role of snoRNAs in the regulation of p53 network remains to be elucidated.

This study demonstrated that SNORD17 promoted HCC progression through a NPM1/MYBBP1A-mediated positive feedback loop upon p53 inactivation. ASOs targeting SNORD17 succeeded to impede tumor growth in mice xenograft models, which provided a potential strategy to control the intractable HCC.

MATERIALS AND METHODS

Patients and tissue specimens

Tongji cohort, including 175 pairs of HCC tissues and adjacent normal liver tissues (ANTs), were obtained from patients with HCC who underwent surgery between 2012 and 2015 at Hepatic Surgery Center, Tongji Hospital of Huazhong University of Science and Technology (Wuhan, China). Inclusion criteria of HCC patients were as follows: definitive HCC diagnosis by pathology based on WHO criteria, with frozen tissues, and with complete follow-up data. The detailed information of all cancer cases was summarized in Supplementary Table S1. The tumor sections had to contain more than 70% tumor cells as determined by a pathologist. The study protocol conformed to the ethical guidelines of the 1975 Declaration of Helsinki and was approved by the Ethics Committee of Tongji Hospital, Tongji Medical College, Huazhong University of Science and Technology (Wuhan, China) (TJ-IRB20210924).

Cell culture

Hepatoma cell line HepG2, human HCC cell lines SK-Hep1, Huh7, and Hep3B (p53-null) and the lentivirus packaging cell line HEK-293T were purchased from China Center for Type Culture Collection (CCTCC, Wuhan, China). All cell lines were cultured in high-glucose DMEM (HyClone) supplemented with 10% fetal bovine serum (FBS) at 37 °C in an atmosphere of 5% CO_2. All cells were examined for short tandem repeat (STR) and mycoplasma infection periodically.

Reagents

Dulbecco's Modified Eagle medium (DMEM), Opti-MEM medium, FBS, and lipofectamine 3000 reagents were obtained as previously described [21]. Doxorubicin (HY-15142), Cycloheximide (CHX) (HY-12320), and MG132 (HY-13259) were all purchased from MedChemExpress. Antibodies and primers used in this study were detailed in Supplementary Table S9.

Peak calling of ChIP-Seq data from the ENCODE project

In order to evaluate whether SNORD17 was actively transcribed, we checked its chromatin features in the chromatin state maps of the HepG2 cell line derived from the Encyclopedia of DNA Elements (ENCODE) project [22, 23]. We merged reads from replicates and wiped off the redundant reads. SNORD17 is evidenced by at least four kinds of epigenetic signatures commonly associated with the activation of transcription (H3K4me1, H3K4me2, H3K4me3, and H3K9Ac) near the transcription start sites.

Real-time PCR (qRT-PCR)

Total RNAs were isolated from cells or human tissues using TRIzol Reagent (Invitrogen, USA) following the manufacturer's instructions. The complementary DNA template was prepared using HiScript III 1st Strand cDNA Synthesis Kit (Vazyme Biotech co., Ltd). ChamQ SYBR Color qPCR Master Mix (Vazyme Biotech co.,ltd) was applied for quantitative real-time PCR analysis according to the manufacture's instruction on a CFX Connect™ Real-Time PCR Detection System (Bio-Rad, Hercules, CA, USA). Each experiment was performed three times independently and the data analysis was performed by $2^{-\Delta\Delta Ct}$ method. GAPDH or U6 was used as endogenous control.

Cell proliferation and colony formation assays

For the cell growth assays, the same amounts of HCC cells were cultured in a 96-well plate. At the indicated time points, the viability of HCC cells was determined by Cell Counting Kit 8 (CCK-8, Wuhan Promoter Biological CO., LTD. #P5090) and measured at 450 nm wavelength with an enzyme-linked immunosorbent assay plate reader (Bio-Tek Elx 800, USA). For each group, the optical density (OD) values were measured by five replicates.

For the colony formation assays, HCC cells were seeded in 6-well plates at a density of 800–1000 cells per well. After 2 weeks, the colonies were fixed with 4% paraformaldehyde and stained with 1% crystal violet. The numbers of colonies >100 μm in diameter were counted using Image J software (NIH Image). Triplicates were performed in each group.

EdU incorporation assay

For the EdU incorporation assay, the same amounts of HCC cells were seeded in 96-well plate (2000 cells/ well) for EdU incorporation assay by using Cell-Light™ EdU Apollo567 In Vitro Imaging Kit (Ribobio, Guangzhou, China) according to the manufacturer's instructions. Briefly, 50 μM EdU solutions (diluted with DMEM) were added into cells and cultured for 2 h. Wash the cells with PBS 1–2 times, and fixed with 4% paraformaldehyde and incubated with 0.5% TritonX-100. Then, cells were stained with 100 μl 1X Apollo solution for 30 min, and then stained nucleus with DAPI. Images were taken with EVOS FL auto imaging system (Life Technologies, USA).

Cell cycle assay

HCC cells (1×10^6) were fixed with 70% ethanol at −20 °C for 24 h, and then stained DNA with propidium iodide (PI) (Jiangsu KeyGEN BioTECH Co., Ltd. # KGA511) containing RNase A. The cells were analyzed by flow cytometry (BD FACS Calibur, BD Biosciences, San Diego, CA, USA). Triplicates were performed for cell cycle profile analysis.

Apoptosis assay

HCC cells (1×10^6) were resuspended in 1× binding buffer and stained with Annexin V-FITC/PI apoptosis detection kit (BD Biosciences, #556547), as suggested by the manufacturer. Cell apoptosis was detected using flow cytometry (BD FACS Calibur, BD Biosciences, San Diego, CA, USA). Triplicates were applied in each group.

Western blot

Cells or human tissues were lysed in RIPA buffer supplemented with EDTA-free protease inhibitor cocktail and a phosphatase inhibitor cocktail (Roche). Bicinchoninic acid (BCA) assay was used to determine the protein concentrations. Subsequently, the cell and tissue lysates were separated by 10% sodium dodecyl sulfate-polyacrylamide gels electrophoresis (SDS-PAGE) and then transferred onto polyvinylidene fluoride (PVDF) membranes. The membranes were blocked in 5% skim milk for 2 h and then incubated overnight with the indicated primary antibody at 4 °C. Next, the membranes were incubated with appropriate secondary antibodies at room temperature for 1 h. The immunoreactive bands were detected using Clarity™ Western ECL substrate (Bio-Rad, USA) and Bio-Rad GelDoc system (Bio-Rad, USA). The antibodies used in this study are provided in Supplementary Table S9.

Immunohistochemistry (IHC)

IHC was performed to evaluate the protein expression of p53, p21, and Ki67 in tumor tissues of mice. The slides were removed from the paraffin in xylene and then rehydrated with ethanol. The slides were performed antigen retrieval with 0.01 M sodium citrate buffer (pH6.0) and then incubated with 3% H_2O_2 for 15 min at room temperature to reduce the non-specific staining, followed by blocking with 5% bovine serum albumin for 60 min. The slides were incubated with primary antibodies overnight at 4 °C. After washing, the slides were incubated with HRP conjugated secondary antibody incubation for 45 min at room temperature. Then the 3-diaminobenzidine tetra-hydrochloride (DAB) was used to detect the antibody binding, and cells were counterstained with hematoxylin. Positive

control and negative control were done each time. Staining scores were evaluated according to the percentage of positive tumor cells and staining intensity score. The IHC signals were scored as previously described [21].

Bioinformatics analysis

Gene Ontology (GO) analysis based on the differential expression genes was performed with the cluster Profiler R package to evaluate the potential biological mechanisms [24]. We visualized significant biological processes using the GO plot R package (Version: 1.0.2; https://cran.r-project.org/web/packages/GOplot/index.html). In order to evaluate the potential mechanism underlying the involvement of SNORD17 in hepatocarcinogenesis, we performed Gene Set Enrichment Analysis (GSEA) analysis (Version: 3.0; http://software.broadinstitute.org/gsea/index.jsp) to identify the difference of the pathways between HCC patients with distinct SNORD17 expression [25]. The hallmark annotated gene set file was accepted for our analysis as the reference. The significance was also based on the threshold of FDR < 0.05.

The CRISPR/Cas9 system

We used a dual gRNA approach to knockout the full-length sequence of SNORD17 by CRISPR/Cas9 system (Ubigene, Guangzhou, China). Briefly, dual gRNA and donor vector were co-transfected into HepG2 cells. One week later, the transfected cells were subject to puromycin (1 μg/ml) selection; surviving cells were sorted into 96-well plates and then expanded into 12-well plates. Potential clones were further verified by genomic PCR and quantitative real-time PCR (qRT-PCR).

SNORD17 overexpression and reintroduction

Sequence from the SNX5 gene was amplified using primers flanking SNORD17 and cloned into the BamHI/SalI sites of pLenti-CMV-Puro plasmid (Addgene #17448) or HindIII/BamHI sites of pcDNA3.1 (Addgene #73066) to generate pLenti-SNORD17 or pcDNA3.1-SNORD17, respectively [26]. pLenti-SNORD17 was applied for packaging of lentivirus and stably overexpressing SNORD17 in HCC cells as described previously [21]. pcDNA3.1-SNORD17 plasmids were transfected into wide-type HCC cells or SNORD17-KO HepG2 cells for transient overexpression of SNORD17. The stable or transient overexpressing efficacy of SNORD17 were evaluated by qRT-PCR.

ASO and siRNA transfection

ASOs were 20 nucleotides long and comprised 10 deoxyribonucleotides flanked by 5-nt 2′-O-methyloxy modified ribonucleotides on both ends. All ASOs were covered by phosphorothioate. HCC cells were cultured in 6-well plates. According to the manufacturer's instructions, when cells reach 70% density, ASOs, siRNAs and their negative control (RiboBio, Guangzhou, China) were transfected with Lipofectamine 3000 (Life Technologies, US).

Luciferase-bearing HCC cells construction

To construct luciferase-bearing HCC cells, firefly luciferase genes were cloned into the EcoRI/XhoI sites of pLVX-Luc-IRES-Neo plasmid (Addgene #128660). Lentiviral vector construction, viral packaging and infection were performed as described previously [21]. 48 h after infection, cells were cultured in 2.5 μg/ml geneticin selection medium for at least 7 days for selecting cells stably expressing luciferase.

Xenograft tumor growth assay

Male BALB/c-nude mice (4 weeks old) were purchased from Beijing HFK Bioscience Co. Ltd. (China) and were maintained under specific-pathogen free conditions. The whole procedure was performed following the "Guide for the Care and Use of Laboratory Animals" (NIH publication 86-23, revised 1985) and was approved by the Committee on the Ethics of Animal Experiments of Tongji Hospital (TJH-201809003). No blinding was performed. To evaluate the tumor growth in vivo, the 4-week-old BALB/c nude male mice were randomized (simple randomization) into groups and 1×10^6 tumor cells were injected subcutaneously into the flanks of nude mice. The volumes were measured every 3 days, and tumor weights were measured after being sacrificed. Tumor volume was calculated according to below: (volume, mm^3) = $0.5 \times$ L (length, mm) $\times$ W^2 (width, mm^2).

To evaluate the tumor growth in vivo, the subcutaneous tumor from HepG2-KO and HepG2-WT cells bearing mice were cut into small pieces (1 mm^3). After the mice were anaesthetized, an incision was created in the upper abdomen and peritoneum. The right lobe of the liver was exposed using a cotton swab and then incised with a scissor. A piece of tumor was transplanted into liver of nude mice (6 mice per group). The abdominal wall was closed. All mice were harvested 6 weeks after transplantation. Tumor volumes and tumor weights were measured as described above.

To evaluate the tumor metastasis in vivo, 1×10^6 HepG2-KO and HepG2-WT cells were injected into the tail veins of mice (10 mice per group) to establish lung metastatic animal model. The development of pulmonary metastases was monitored by bioluminescence imaging. All mice were harvested 8 weeks after transplantation.

All tumors were collected and applied for H&E staining and histologic evaluation (paraffin section).

Immunofluorescence (IF)

Cells were cultured on coverslips in 12-well plate. Cells were fixed with 4% paraformaldehyde for 15 min at room temperature, following permeabilized with 0.5% Triton X-100 for 10 min. Cells were incubated with the indicated primary antibody overnight at 4 °C after blocking with 5% bovine serum albumin for 1 h. Appropriate secondary antibody (FITC or DyLight549-conjugated Goat anti-Mouse IgG and DyLight549 or DyLight649-conjugated Goat anti-Rabbit IgG) was used to incubate cells for 1 h in 37 °C. DAPI counterstained nuclei. Images were taken with confocal laser-scanning microscopy on the Nikon Digital ECLIPSE C1 system (Nikon Corporation).

Fluorescence in situ hybridization (FISH)

Cells were cultured on coverslips in 12-well plates. cy3-labeled SNORD17 detection probe was purchased from Ribobio (Guangzhou, China). FISH was performed with Ribo™ Fluorescent In Situ Hybridization Kit (Ribobio, Guangzhou, China) according to the manufacturer's instructions. Images were taken with confocal laser-scanning microscopy on a Nikon Digital ECLIPSE C1 system (Nikon Corporation).

RNA library construction and sequencing

Total RNA was extracted using TRIzol reagent (Invitrogen, CA, USA) following the manufacturer's procedure. Bioanalyzer 2100 and RNA 6000 Nano LabChip Kit (Agilent, CA, USA) analyzed the total RNA quantity and purity with RIN number >7.0. Approximately 10 μg of total RNA was used to deplete ribosomal RNA according to the Epicenter Ribo-Zero Gold Kit (Illumina, San Diego, USA). Following purification, the poly(A)− or poly(A)+ RNA fractions was fragmented into small pieces using divalent cations under elevated temperature. Then the cleaved RNA fragments were reverse-transcribed to create the final cDNA library following the protocol for the mRNA-Seq sample preparation kit (Illumina, San Diego, USA), the average insert size for the paired-end libraries was 300 bp (±50 bp). And the paired-end sequencing was then performed by Novogene corporation (Beijing, China) using an Illumina platform.

RNA pull-down assay

For RNA pull-down, 4×10^7 HepG2 cells were lysed in 1 mL RIP buffer, and cell lysates were cleared by centrifuging at 13,000 rpm for 10 min at 4 °C. 100 pmol biotinylated RNA probes against SNORD17 or SNORD21 were incubated with cell lysates for 4 h at 37 °C. A total of 50 μl washed Streptavidin magnetic beads (Invitrogen) were added to each binding reaction and further incubated for 1 h at room temperature. Beads were collected post washed with RIP washing buffer for five times, and followed by SDS-PAGE or mass spectrometry analysis. The sequence of probes was provided in Supplementary Table S9.

RNA-binding protein immunoprecipitation (RIP)

According to the manufacturer's instructions, RNA immunoprecipitation assay was performed using Megna RIP RNA-binding Protein Immunoprecipitation Kit (Millipore). Briefly, 4×10^7 HepG2 cells were lysed in 200 μL RIP buffer, and cell lysates were cleared by centrifuging at 13,000 rpm for 10 min at 4 °C. 20 μL cleared lysates were set aside as input and stored in −80 °C. Then cleared lysates were incubated with beads that were pre-coated with specific antibodies antibody overnight at 4 °C. Beads were washed 7 times with RIP washing buffer. The beads were resuspended in 2× loading buffer to elute proteins or resuspended in TRIzol extract RNA after being treated with DNase and Proteinase K. SNORD17 were detected by qRT-PCR after reverse transcription.

Co-immunoprecipitation (Co-IP)

1×10^7 Cells was harvested and suspended in 1 ml IP-lysis buffer (50 mM Tris-HCl, 150 mM NaCl, 1% Triton X-100, 1 mM EDTA, 10% glycerol, and protease inhibitor cocktail, pH7.4), and cell lysates were cleared by centrifuging at 13,000 rpm for 10 min at 4 °C. After being pre-cleared with 30 μl protein

G-conjugated agarose (GE Healthcare Life Sciences) for 4 h, the cell lysates were incubated with a specific antibody overnight at 4 °C. Then the cell lysates were immunoprecipitated with 25 µl protein G-conjugated agarose for 4 h at 4 °C, followed by washed for 5–7 times with IP-wash buffer (50 mM Tris-Cl, 300 mM NaCl, 1% Triton X-100, 1 mM EDTA, pH7.4).

Ubiquitination assays

To analyze the ubiquitination of p53 in indicated HCC cells, cells were treated with 20 µM MG132, a proteasome inhibitor, for 4 h, then whole-cell lysis was applied foe immunoprecipitation with anti-p53 antibody and further analyzed by immunoblot with anti-ubiquitin antibody.

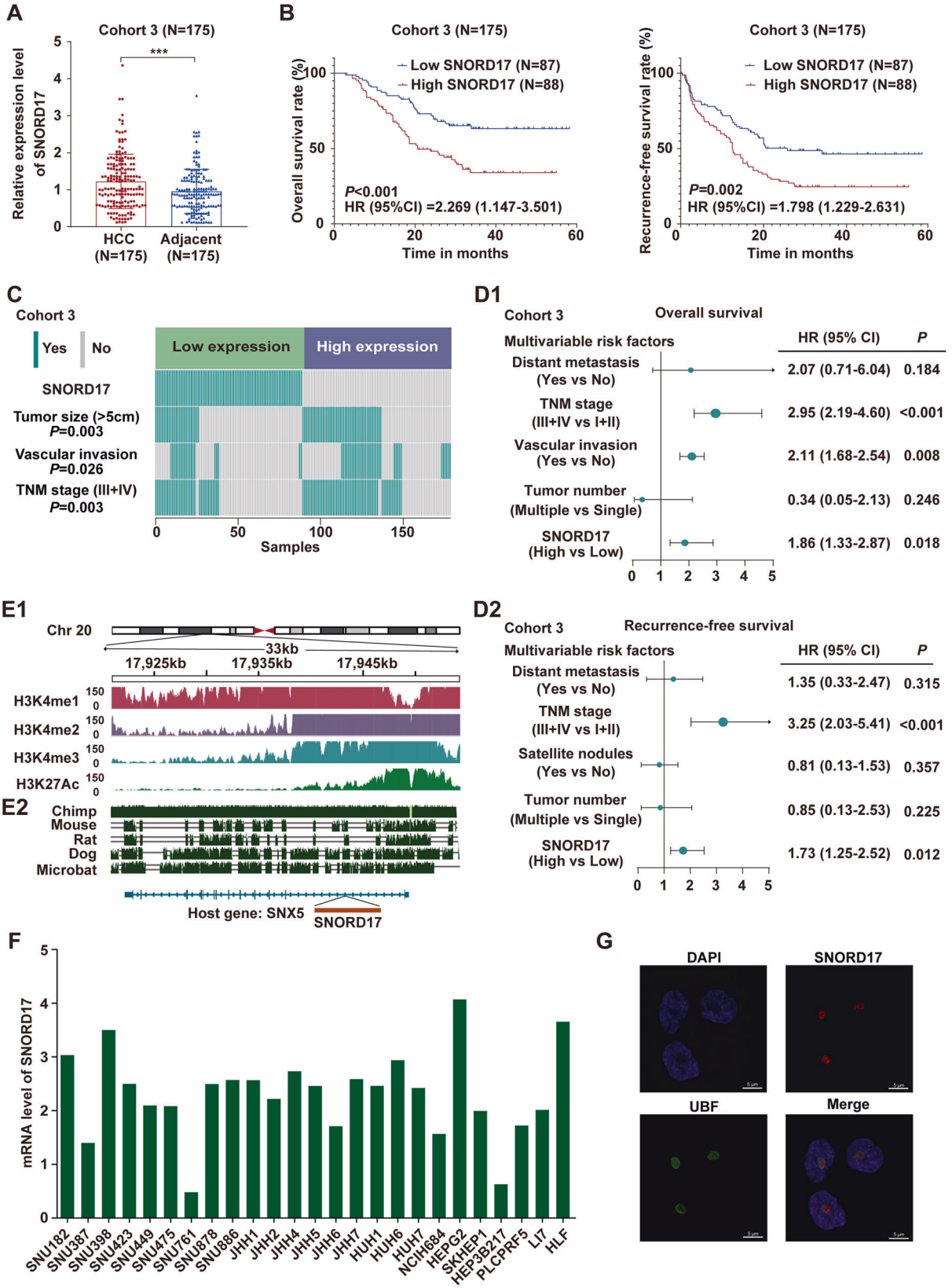

Fig. 1 Identification of SNORD17 as a clinically relevant snoRNA in HCC. A qRT-PCR analysis of SNORD17 expression in HCC tissues and adjacent non-tumor tissues of patients in HCC cohort 3. Data are shown as mean ± SEM. **B** Kaplan–Meier analysis of the correlation between SNORD17 expression and OS (left) or RFS (right) in HCC cohort 3. **C** Chi-square analysis of the relevance of SNORD17 expression with tumor size, vascular invasion, and TNM stage in cohort 3. **D** Multivariate analyses of factors associated with OS (D1) and RFS (D2) in cohort 3. All the bars correspond to 95% confidence intervals. **E** Chromatin signatures of H3K4me1, H3K4me2, H3K4me3, and H3K27Ac modification in SNORD17 gene locus in HepG2 cells (GSE26320) (E1) and chromatin conservation at the locus of SNORD17 (E2). **F** Relative SNORD17 expression levels in 25 HCC cell lines analyzed by the Cancer Cell Line Encyclopedia. **G** FISH assay for SNORD17 in HepG2 cells. Red: SNORD17; blue: DAPI; green: UBF (nucleolar marker). The statistical significance was determined by Student's two-tailed *t* test (**A**), log-rank test (**B**), and chi-square (**C**). In (**D**), the effects of variables on survival rate were determined by multivariate Cox proportional hazards modeling. ***$P < 0.001$. HR hazard rate, 95% CI 95% confidence intervals.

Chromatin immunoprecipitation (ChIP)

ChIP assay was performed using SimpleChIP® Plus Sonication Chromatin IP Kit (Cell Signaling Technology #56383). Briefly, 1×10^7 HepG2 cells were cross-linked with 1% formaldehyde for 20 min. Cells were lysed in 1 mL ChIP Sonication Cell Lysis Buffer, and cell lysates were sheared with a sonicator microprobe for 4 rounds of 15, 1 s pluses at output level 6. The sheared chromatin was incubated with the antibody overnight at 4 °C, and then incubated with beads for 2 h at 4 °C. The beads were washed for five times with wash buffer, followed by DNA isolation for qRT-PCR or PCR reactions.

Luciferase reporter assay

SNORD17 is located between the first and second exon of the SNX5 gene and share the same promoter. Indeed, SNORD17 expression positively correlates with the expression of SNX5 in HCC tissues (Supplementary Fig. S2F). To identify the promoter region of the gene (SNX5), we identified RNA polymerase II (RNAPII) occupancy and chromatin features of active transcription within the gene and in the upstream intergenic region (~20 kilobases) using the UCSC Genome Browser database (http://genome.ucsc.edu;). ChIP sequencing datasets revealed that RNAPII peaks and transcriptional regulatory elements were present in the region spanning approximately −200 and +1500 base pairs (bp) from the transcription start site (TSS) of SNX5. We cloned the genomic sequence located between −200 and +2000 base pairs (bp) from the transcription start site (TSS) and site-directed mutagenesis into the KpnI/XhoI sites of pGL4.17[luc2/Neo] plasmid (Promega). According to the manufacturer's instructions, luciferase reporter assays were performed (Promega, Madison, WI, USA). The relative luciferase activity was determined by a GloMax 20/20 Luminometer (Promega). Firefly luciferase activity was normalized to Renilla activity.

Isolation of nucleoli

Nucleoli isolation in HepG2 cells was performed as previously described [27]. 3×10^7 cells were collected and suspended in ice-cold NSB (10 mM Tris·Cl, pH 7.4, 10 mM NaCl, 1.5 mM $MgCl_2$, 1 tablet of Boehringer complete protease inhibitor for 50 ml) to 15 times the residual volume (RV) for 30 min on ice. 20 µl lysates were taken out for total RNA extraction or protein detection. Appropriate volume of NP-40 solution was added in the homogenate to obtain a final concentration of 0.3%, then transferred the homogenate (~15 ml) immediately to a 0.4 mm clearance 15 ml Dounce homogenizer for gentle separation of nuclei and cytoplasm. The homogenate was centrifuged for 5 min at $1200 \times g$, 4 °C, and collected the supernatant that contains the cytoplasmic fraction. To fractionate nuclear fractions, the pellet was fractionated by 250 mM sucrose solution and 880 mM sucrose solution and resuspended with 10 RV 340 mM sucrose solution containing 5 mM $MgCl_2$. To prepare nucleoplasm and nucleolar fractions, the nucleus was broken by a sonicating nuclear fraction. 10 RV of 880 mM sucrose was added to the bottom of sonicated nuclear fraction and then centrifuged 20 min at 2000 rpm, 4 °C to pellet nucleoli. The supernatant was collected as nucleoplasm fraction, and the pellet was resuspended in a minimal volume 0.34 M sucrose buffer as nucleolar fraction for analysis.

p53 mutation screening

According to a previous report, the highly conserved exons 5 to 8 of the p53 gene were screened [16]. The primers used in PCR and sequencing were listed in Supplementary Table S9. A total of 109 patients in HCC Cohort 3 were screened for p53 mutations by PCR followed by Sanger sequencing (ABI Prism 3730).

SNORD17 ASO treatment for tumor bearing mice

ASO was dissolved in sterile PBS, and oligonucleotide concentration was determined before aliquoting for storage at −80 °C. No blinding was performed. Subcutaneous xenograft and orthotopic xenograft tumor models were established as described above. Mice were randomized (simple randomization) into two groups and treated with intratumor injections or intraperitoneal injections of SNORD17 ASO or control ASO at 10 mg/kg daily for 5 days, followed by 1 day off treatment for a total of 18 days. The tumor volumes were measured every 3 days, and tumor weights were measured after being sacrificed. Tumor volume was calculated according to the following formula: volume (mm^3) = 0.5 × L (length, mm) × W^2 (width, mm^2). All tumors were collected and applied for H&E staining and histologic evaluation (paraffin section).

Statistical analysis

The results were expressed as mean ± standard error of mean (SEM). Statistical analyses were performed using SPSS (standard V.16.0; IBM Corporation, Armonk, NY). Data were tested for homogeneity of variances and normality. The Chi-square (χ^2) test was used for comparison of patient characteristics and SNORD17 expression level. Crude relative risks (RRs) of death associated with SNORD17 expression and other predictor variables were estimated by the univariate Cox proportional hazards regression model. A multivariate Cox model was constructed to estimate the adjusted RR for SNORD17 expression. Overall survival (OS) and recurrence-free survival (RFS) was evaluated by the Kaplan–Meier survival curve and the Log-rank test. The Mann–Whitney *U* test or Student *t* test was performed to compare the variables of two groups. Statistical tests and *P*-values were two-sided. $P < 0.05$ was taken as statistically significant.

RESULTS

Identification of SNORD17 as a clinically relevant snoRNA related to HCC

To identify snoRNAs that are correlated with the clinical features of HCC, we analyzed two HCC patient cohorts from the Gene Expression Omnibus (GEO) database (Supplementary Fig. S1A). A total of 54 snoRNAs were significantly differentially expressed in HCC tissues compared to normal tissues in both cohorts (Supplementary Fig. S1B; Supplementary Table S2). Kaplan–Meier analyses showed that 7 out of these 54 snoRNAs were correlated with the clinical outcomes of HCC patients, and high expressions of these snoRNAs were significantly associated with poor prognoses in cohort 2 (Supplementary Fig. S1C1, C2). To validate these results, we analyzed the expression levels of these 7 snoRNAs in HCC tissues and ANTs from 175 patients enrolled in Tongji Hospital (cohort 3, Supplementary Table S1). qRT-PCR revealed that 3 out of the 7 snoRNAs were upregulated in HCC tissues compared to ANTs (Fig. 1A; Supplementary Fig. S1D). Kaplan–Meier analyses of cohort 3 showed that only high expression of SNORD17 was significantly associated with shorter OS and RFS of patients with HCC (Fig. 1B; Supplementary Fig. S1E1, E2). In addition, high expression of SNORD17 in HCC was positively correlated with larger tumor size, vascular invasion and advanced TMN stage in cohort 3 (Fig. 1C; Supplementary Table S3). Univariate and multivariate regression analyses confirmed that higher SNORD17 expression was independently associated with

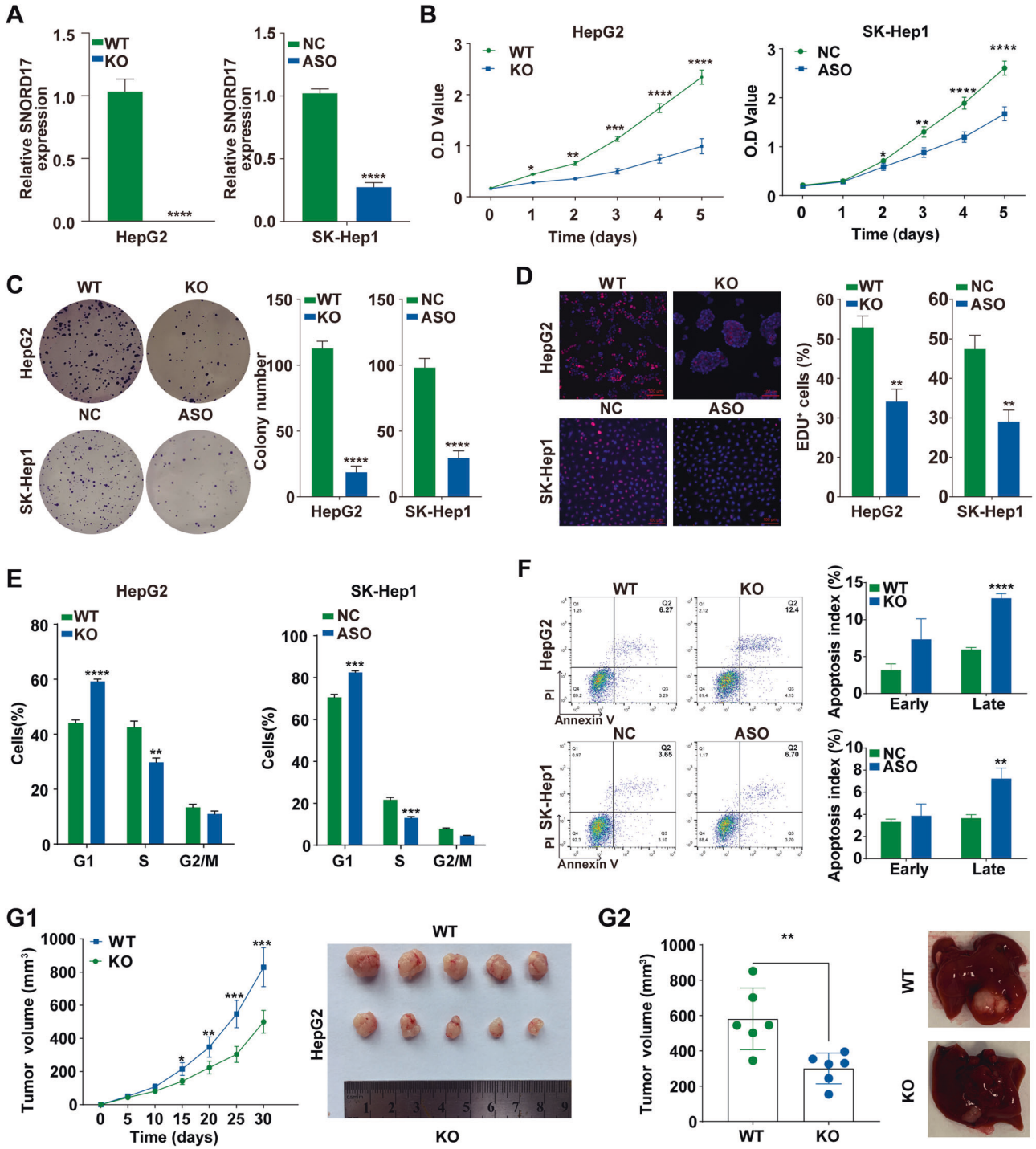

Fig. 2 SNORD17 promotes the proliferation, cell cycle progression, and apoptosis resistance of HCC cells in vitro and in vivo. A The expression level of SNORD17 was determined by qRT-PCR. SNORD17 was silenced in HepG2 and SK-Hep1 cells using CRISPR-Cas9 or ASO, respectively. **B** CCK8 assay (cell counting assay) in SNORD17-silence cells. **C** Representative images of cell colonies and quantification of colony numbers in SNORD17-silence cells. **D** Representative images of EDU assays and quantification of EDU^+ cells in SNORD17-silence cells. **E** Cell cycle profiles in the indicated cells. **F** Apoptosis rates in SNORD17-silence cells were analyzed by flow cytometry (Early apoptosis: Annexin V positive/PI negative; late apoptosis: Annexin V positive/PI positive). **G** Subcutaneous and orthotopic tumor growth assays in mice injected with SNORD17-knockout HepG2 cells. (G1) Growth curves and macroscopic view of subcutaneous tumors in the indicated groups ($n = 5$ mice/group); Data are shown as mean ± SEM. (G2) Tumor volume and representative macroscopic views of orthotopic tumors in the indicated groups ($n = 6$ mice/group). Data are shown as mean ± SEM. In (**A**–**F**), data are shown as mean ± SEM; $n = 3$ independent experiments. In (**A**–**G**), the statistical significance was determined by Student's two-tailed t test. $^*P < 0.05$; $^{**}P < 0.01$; $^{***}P < 0.001$; $^{****}P < 0.0001$. WT wild type, KO SNORD17 knocked out, NC negative control ASOs, ASO anti-SNORD17 ASOs, OD optical density.

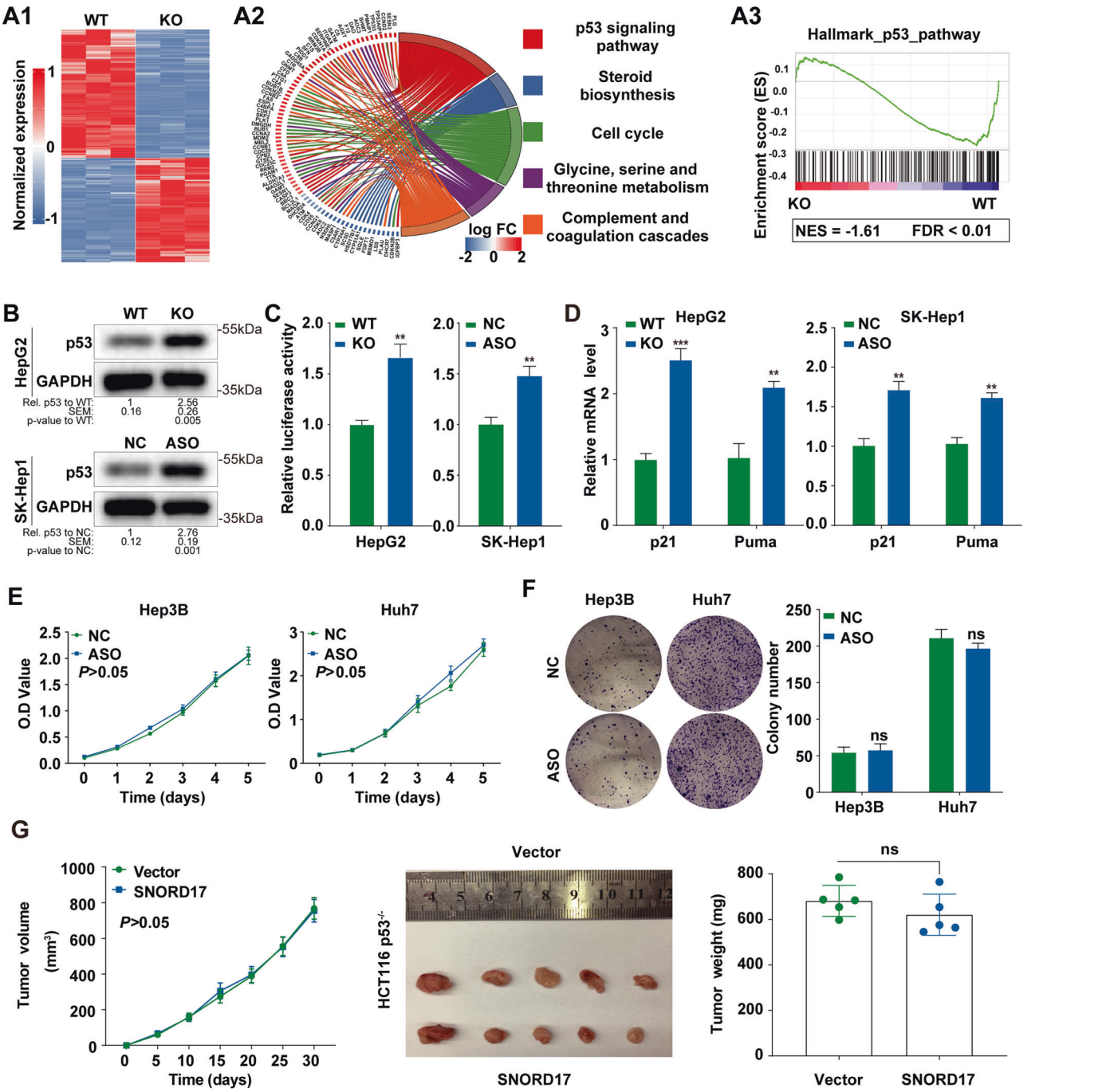

Fig. 3 SNORD17 affects p53-dependent HCC cell growth. A Identification of downstream effectors of SNORD17. (A1) Heatmap of the differentially expressed genes between SNORD17-knockout and wild-type HepG2 cells (left) ($n = 3$ samples/group). (A2) The top five KEGG pathway terms significantly enriched in the SNORD17 regulated genes (middle) ($n = 3$ samples/group). (A3) GSEA plots of p53 pathway-related signatures in SNORD17-knockout HepG2 cells *versus* control cells ($n = 3$ samples/group). **B** The protein levels of p53 were detected using western blot in SNORD17-silence cells. Representative immunoblot of $n = 3$. **C** Dual-luciferase reporter assays for p53 transcriptional activities in SNORD17-silence cells. **D** qRT-PCR analysis of p21 and Puma in SNORD17-silence cells. **E** CCK8 assay was performed in Hep3B (p53-null) and Huh7 (p53-mutant) after transfection with anti-SNORD17 ASO or negative control (NC) ASOs for 24 h. **F** Colony formation assays were performed in Hep3B and Huh7 cells after transfection with anti-SNORD17 ASOs (ASO) or negative control ASOs (NC) for 24 h. **G** Growth curves, macroscopic view and weights of subcutaneous tumors in mice bearing HCT116 $p53^{-/-}$ cells with SNORD17 overexpressed ($n = 5$ mice/group). Data are shown as mean ± SEM. In (**C**–**F**), data are shown as mean ± SEM; $n = 3$ independent experiments. The statistical significance was determined by Student's two-tailed t test (**C**–**G**). $^{**}P < 0.01$; $^{***}P < 0.001$; ns no significance. WT wild type, KO SNORD17 knocked out, NC negative control ASOs, ASO antisense oligonucleotides, FC fold change, NES normalized enrichment score, FDR false discovery rate.

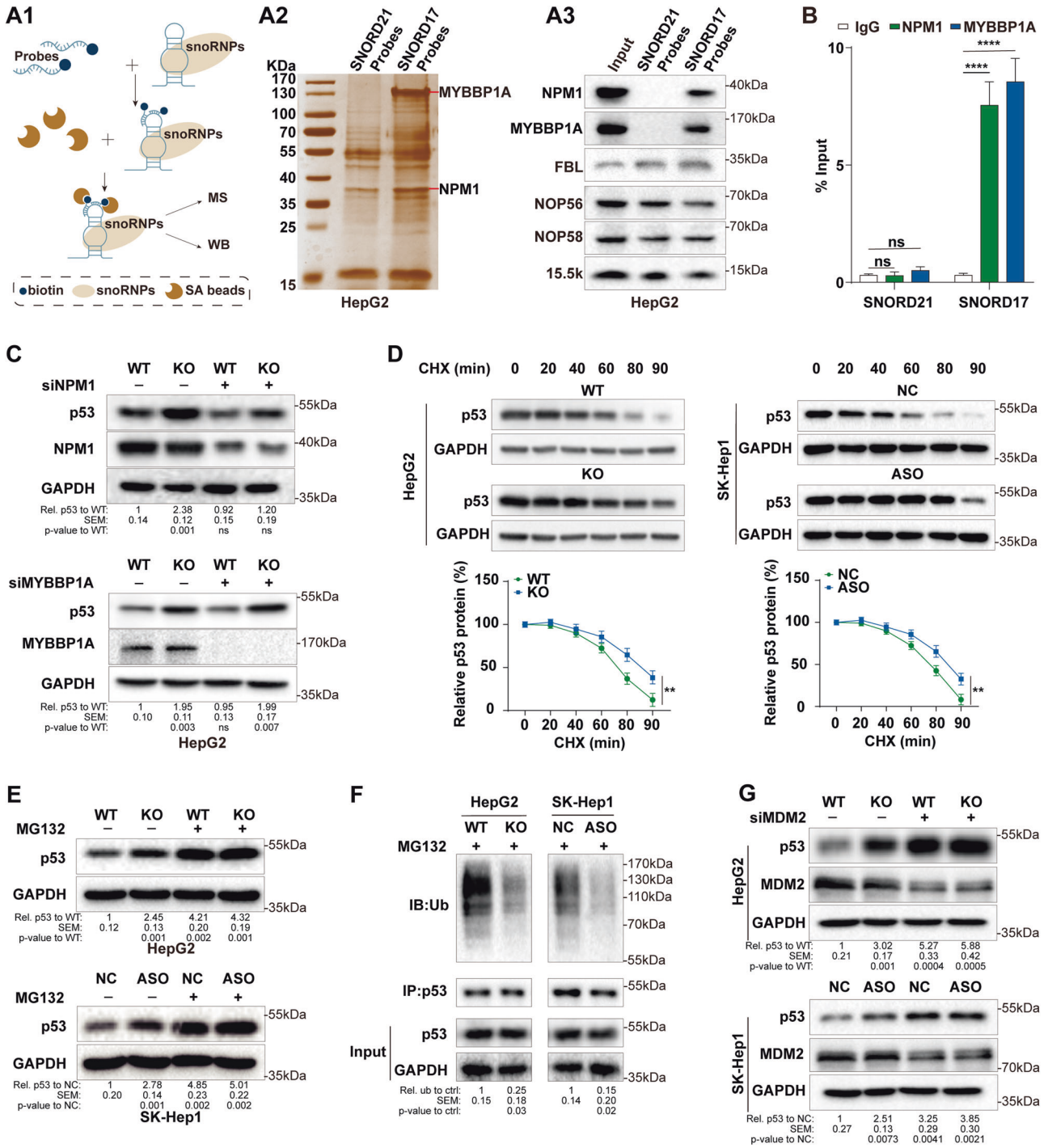

Fig. 4 SNORD17 promotes MDM2-mediated p53 ubiquitination *via* NPM1. A RNA pull-down assay in HepG2 cells. (A1) Flow chart of the strategy for RNA pull-down assay. (A2) Silver staining of proteins enriched by SNORD17 or SNORD21 (negative control) in HepG2 cells. The arrow indicated the additional bands that were enriched by SNORD17 as compared to control. (A3) Western blot analysis of MYBBP1A and NPM1 abundances in SNORD17 pull-down precipitates in HepG2 cells. FBL, Nop56, Nop58, and 15.5k were taken as positive control. **B** qRT-PCR analysis of SNORD17 and SNORD21 level in complexes enriched by RNA immunoprecipitation assays of NPM1 and MYBBP1A in HepG2 cells. Data are shown as mean ± SEM; $n = 3$ independent experiments. **C** Western blot assay for p53 expression in SNORD17-silence HepG2 cells with or without transfection of NPM1 or MYBBP1A siRNA. **D** Western blot analysis and quantification of p53 level in SNORD17-silence cells treated by CHX (100 μg/ml) at the indicated time interval. Error bars represent the mean ± SEM of three independent experiments. **E** The protein levels of p53 were detected using western blot in SNORD17-silence cells with or without treatment of 20 μM MG132. **F** The ubiquitination of p53 protein was detected by immunoprecipitation with anti-p53 antibody in SNORD17-silence cells after treatment of MG132 (20 μM) for 4 h. **G** The protein levels of p53 were detected using western blot in SNORD17-silence cells with or without transfection of MDM2 siRNA. In all panels, a representative blot of three independent experiments performed is shown. The statistical significance was determined by Student's two-tailed *t* test (**B**). ****$P < 0.001$; WT wild type, KO SNORD17 knocked out, NC negative control ASOs, ASO anti-SNORD17 ASOs, siRNA small interference RNA, Ub ubiquitin, IB immunoblotting, IP immunoprecipitation; **$P < 0.01$.

shorter OS and RFS (Fig. 1D1, D2; Supplementary Fig. S1F; Supplementary Tables S4, S5).

By examining the histone modification profiles of HepG2 cells in the ENCODE, we identified four kinds of epigenetic signatures in the SNORD17 promoter region (Fig. 1E1), indicating its active transcription status in HCC cells. SNORD17 also exhibits a high degree of evolutionary conservation across species (Fig. 1E2). In HCC cell lines profiled in the Cancer Cell Line Encyclopedia Project [28], we found that SNORD17 was generally highly expressed (Fig. 1F). qRT-PCR showed that the levels of SNORD17 in the indicated HCC cell lines were comparable (Supplementary Fig. S2A). FISH analysis showed that SNORD17 was almost exclusively localized in the nucleoli of HepG2 cells (Fig. 1G). These results indicate that SNORD17 is a clinically relevant snoRNA in HCC.

SNORD17 promotes the proliferation, cell cycle progression and apoptosis resistance of HCC cells in vitro

To elucidate the function of SNORD17 in HCC, we knocked out (KO) SNORD17 expression in HepG2 cells (Fig. 2A; Supplementary Fig. S2B). qRT-PCR revealed that SNORD17 depletion did not affect the mRNA expression of adjacent genes, or the protein expression and subcellular localization of host gene SNX5 (Supplementary Fig. S2C–E) [29]. Additionally, we knocked down SNORD17 expression in SK-Hep1 cells *via* ASO transfection (Fig. 2A). Knockout or knockdown of SNORD17 in HCC cell lines significantly inhibited cell proliferation, colony formation and G1/S phase transition (Fig. 2B–E). Vice versa in SNORD17 overexpressed HCC cells (Supplementary Fig. S3A–E). Western blot analysis showed that depleted or knockdown of SNORD17 downregulated the

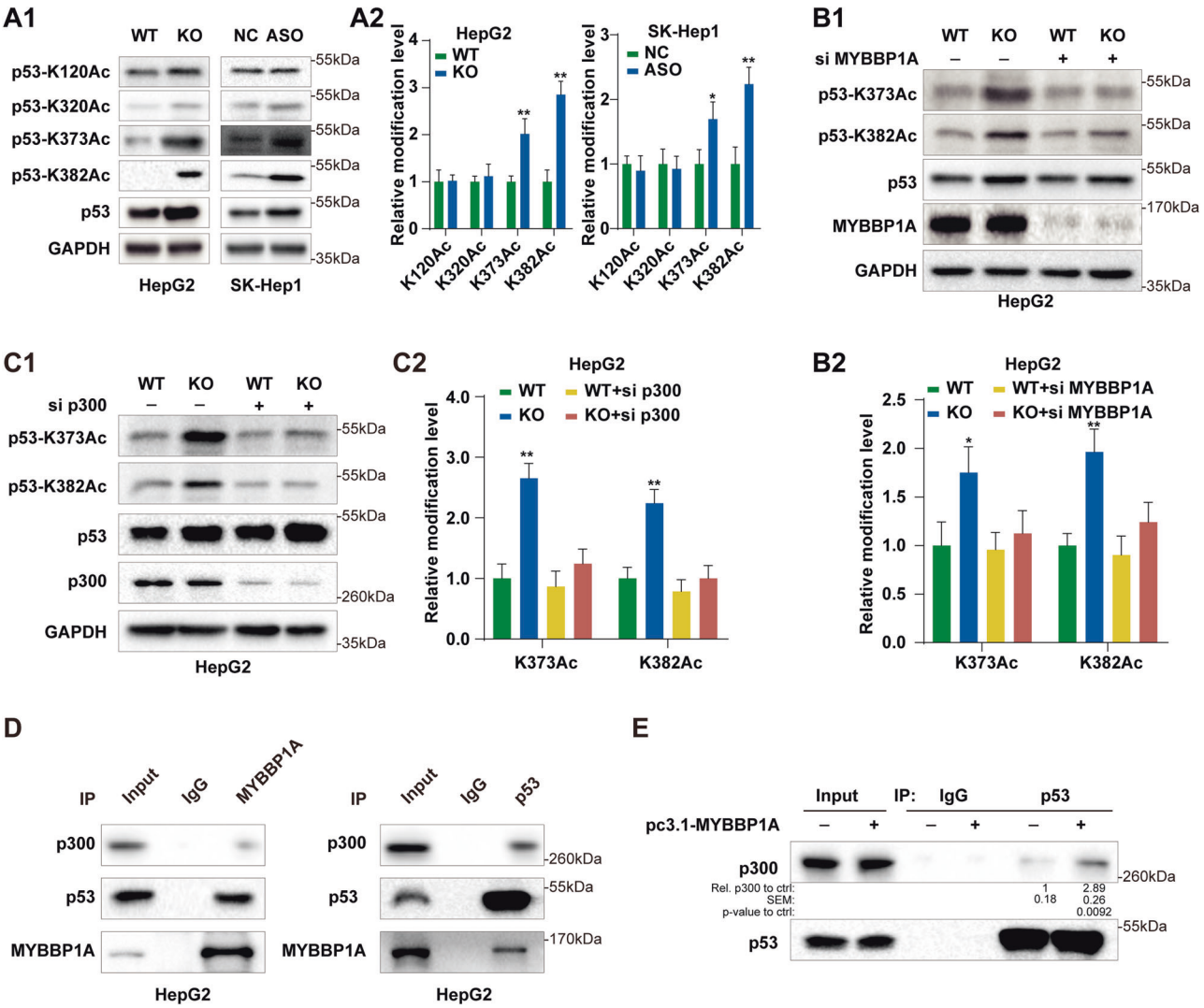

Fig. 5 SNORD17 promotes p300-mediated p53 acetylation *via* MYBBP1A. A Western blot analysis and quantification of acetylated p53 level in SNORD17-silence cells. (A1) The acetylated sites of p53 were detected at K120, K320, K373 and K382 sites. (A2) Quantification of acetylation levels of the p53 protein in the indicated sites. Data are shown as mean ± SEM; $n = 3$ independent experiments. **B** Western blot analysis and quantification of acetylated p53 at K373/382 were detected in SNORD17-depletion HepG2 cells with or without transfection of MYBBP1A siRNA (B1). Quantification of acetylation levels of the p53 protein in the indicated sites (B2). Data are shown as mean ± SEM; $n = 3$ independent experiments. **C** Western blot analysis and quantification of acetylated p53 at K373/382 were determined in SNORD17-depletion HepG2 cells with or without transfection of p300 siRNA (C1). Quantification of acetylation levels of the p53 protein in the indicated sites (C2). Data are shown as mean ± SEM; $n = 3$ independent experiments. **D** The interaction of endogenous MYBBP1A with p53 and p300 was detected by Co-IP assays in HepG2 cells. **E** Cells were transfected with pcDNA3.1-MYBBP1A plasmids (pc3.1-MYBBP1A) to overexpress MYBBP1A. Co-IP assays detected the interaction of endogenous p300 and p53 in MYBBP1A overexpression HepG2 cells. In (A2, B2, and C2), the band's intensities of the acetylated p53 proteins were normalized to p53 protein level. The statistical significance was determined by Student's two-tailed *t* test. WT wild type, KO SNORD17 knocked out, NC negative control ASOs, ASO anti-SNORD17 ASOs, siRNA small interference RNA, IB immunoblotting, IP immunoprecipitation, $^{*}P < 0.05$; $^{**}P < 0.01$.

expression of the critical G1 cell cycle regulators cyclin D1 and cyclin-dependent kinase 4 (CDK4) while upregulating the expression of G1 cell cycle inhibitors p21 and p27 (Supplementary Fig. S3F). Vice versa in HCC cells with SNORD17 overexpression (Supplementary Fig. S3F). Additionally, flow cytometry analysis showed an increase in the number of late apoptotic cells among HepG2-KO and ASO-transfected SK-Hep1 cells compared with their respective controls (Fig. 2F). Overexpression of SNORD17 decreased DOX-induced apoptosis in HepG2 and SK-Hep1 cells (Supplementary Fig. S3G). At the same time, western blot analysis

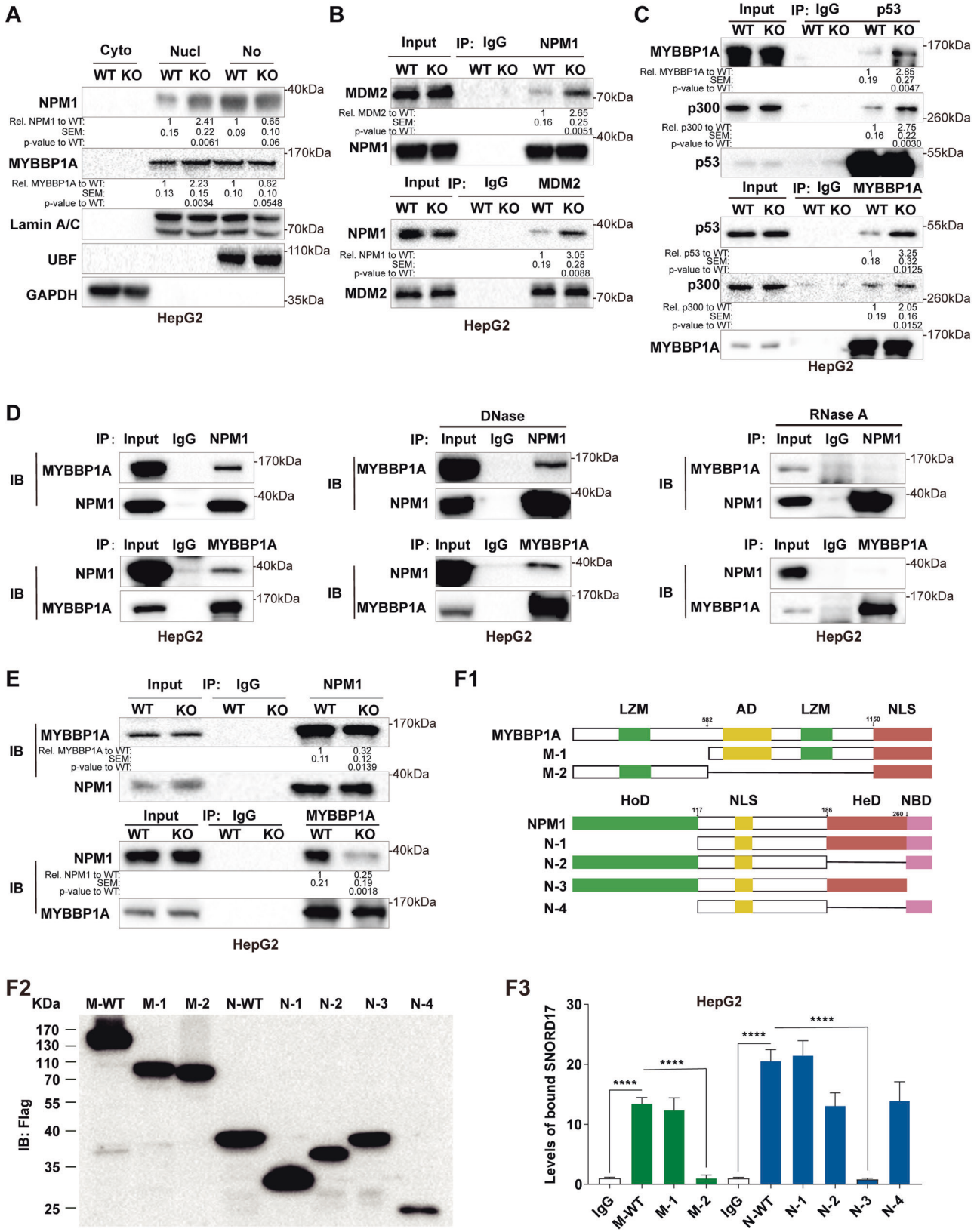

Fig. 6 SNORD17 anchors NPM1 and MYBBP1A in the nucleolus by simultaneous binding with them. A Total protein lysate from HepG2 cells was separated into cytoplasmic (Cyto), nucleoplasmic (Nucl), and nucleolar (No) fractions. The protein levels of NPM1 and MYBBP1A were detected in these fractions using western blot. UBF, Lamin A/C and GAPDH serves as an internal reference for the nucleolar nucleoplasmic and cytoplasm, respectively. **B** Co-IP assays detected the interaction of endogenous NPM1 and MDM2 in SNORD17-depletion HepG2 cells. **C** Co-IP assays detected the interaction of endogenous MYBBP1A, p53, and p300 in SNORD17-depletion HepG2 cells. **D** Co-IP assays detected the binding of endogenous NPM1 and MYBBP1A in HepG2 cells with different treatments. Cellular lysates from HepG2 cells were treated with DNase (middle), RNase A (right), or without any treatment (left). **E** Co-IP assays detected the interaction of endogenous NPM1 and MYBBP1A in SNORD17-depletion HepG2 cells. **F** RNA immunoprecipitation (RIP) assays for the binding abilities between SNORD17 with truncates of NPM1 and MYBBP1A. (F1) Schematic diagram of the plasmids encoding flag-tagged full-length or the truncated mutants of NPM1 and MYBBP1A. (F2) Plasmids encoding flag-tagged full-length or truncated mutants of NPM1 and MYBBP1A were transfected into HepG2 cells, and their expression efficacies were detected by western blot. (F3) qRT-PCR was performed to determine the levels of SNORD17 in the RIP precipitates in HepG2 cells transfected with the indicated plasmids. Data are shown as mean ± SEM; $n = 3$ independent experiments. In all panels, a representative blot of three independent experiments performed is shown. The statistical significance was determined by Student's two-tailed *t* test (F3). ****$P < 0.0001$; WT wild type, KO SNORD17 knocked out, IB immunoblotting, IP immunoprecipitation, LZM leucine zipper-like motifs, AD the acidic domain, NLS nucleolar localization sequence, HeD heterodimerization domain, HoD homodimerization domain, NBD nucleic acid binding domain.

showed that impairing SNORD17 significantly increased the protein levels of the active forms of caspase-3, caspase-9, and poly adenosine diphosphate-ribose polymerase (PARP), while overexpression of SNORD17 had the opposite effects (Supplementary Fig. S3H). Consistent results were obtained in HepG2 cells with SNORD17 knocked down *via* ASO transfection (Supplementary Fig. S4A–E).

SNORD17 promotes the tumorigenesis and metastasis of HCC in vivo

The subcutaneous tumor volume and weight in mice injected with HepG2-KO cells was significantly smaller and lower than those in control mice, respectively (Fig. 2G1; Supplementary Fig. S5A). Ki67 staining and terminal deoxynucleotidyl transferase-mediated deoxyuridine triphosphate nick-end labeling (TUNEL) assays of the subcutaneous tumors revealed a consistent effect of SNORD17 on cell proliferation and apoptosis in vivo (Supplementary Fig. S5B, C). Conversely, overexpression of SNORD17 in HepG2 cells promoted tumor growth in the subcutaneous xenograft mouse model (Supplementary Fig. S5D–G).

We further examined the role of SNORD17 in HCC growth by establishing an orthotopic xenograft tumor model using subcutaneous xenograft tumors derived from HepG2-WT and HepG2-KO cells. The results showed that knockout of SNORD17 in HepG2 cells significantly decreased the orthotopic liver tumor volume and tumor weight compared to controls (Fig. 2G2; Supplementary Fig. S5H). Moreover, in a lung metastasis model, there were reduced lung metastases in mice injected with HepG2-KO cells than those injected with control cells (Supplementary Fig. S5I). These data indicated that SNORD17 promoted the tumorigenesis and metastasis of HCC in vivo.

p53 mediates the impact of SNORD17 on HCC cell growth

To explore the molecular mechanisms by which SNORD17 promotes the progression of HCC, we performed mRNA expression profiling to examine the gene expression changes after knocking out SNORD17 in HepG2 cells (Fig. 3A1; Supplementary Table S6). KEGG and GSEA analyses of the differentially expressed genes revealed that the most enriched pathway was the p53 signaling pathway, and it was negatively correlated with SNORD17 expression (Fig. 3A2, A3). These differentially expressed genes involved in the p53 pathway were relevant to the cell cycle, apoptosis and metastasis (Supplementary Fig. S6A). Western blot showed that knockout or knockdown of SNORD17 upregulated p53 expression in HepG2 and SK-Hep1 cells (Fig. 3B), whereas SNORD17 overexpression led to decreased p53 protein levels (Supplementary Fig. S6B). Consistently, IHC staining exhibited that the p53 levels in the subcutaneous tumors of mice were negatively correlated with the expression of SNORD17 (Supplementary Fig. S6C). In addition, luciferase reporter assays indicated that knockout or knockdown of SNORD17 significantly enhanced endogenous p53 transcriptional activity (Fig. 3C). The mRNA expression of p21 and Puma, downstream effectors of p53, were also suppressed by SNORD17 in HCC cells (Fig. 3D; Supplementary Fig. S6D). Furthermore, the inhibited proliferation ability in SNORD17-knockdown cells was diminished when p53 was knocked out or knocked down (Supplementary Fig. S6E, F1, F2). While, SNORD17 did not affect the proliferation and colony formation abilities of Huh7 (p53-mutant) and Hep3B (p53-null) cells (Fig. 3E, F; Supplementary Fig. S6G–I), and overexpression of SNORD17 in HCT116 $p53^{-/-}$ cells failed to promote tumor growth (Fig. 3G; Supplementary Fig. S6J). These finding suggests that the oncogenic role of SNORD17 in HCC depends on p53.

SNORD17 promotes MDM2-mediated p53 ubiquitination *via* NPM1

To elucidate the mechanism by which SNORD17 regulates the expression of p53, we sought to define the protein interactome of SNORD17 by endogenous RNA pull-down assay. Another C/D box snoRNA, SNORD21, which does not correlate with HCC (Fig. 4A1; Supplementary Fig. S7A, B), was used as negative control. Except for the protein detected in both group, such as the 'core' snoRNP proteins fibrillarin, NOP58, NOP56 and 15.5k (Supplementary Table S7) [10], 19 proteins were found bound specifically to SNORD17 in the mass spectrum assay (Supplementary Table S8). Among them, MYBBP1A and NPM1 stood out because they were the top two enriched proteins and were previously reported be involved in the regulation of p53 (Fig. 4A2; Supplementary Table S8) [30, 31]. Western blot confirmed that the enrichment of NPM1 and MYBBP1A in anti-SNORD17 precipitates (Fig. 4A3). RIP assays confirmed that MYBBP1A and NPM1 interacted with SNORD17 reciprocally (Fig. 4B). IF images also displayed the colocalization of SNORD17 with MYBBP1A or NPM1 in the nucleoli (Supplementary Fig. S7C). Furthermore, we found that the elevation of p53 protein levels in SNORD17-knockdown cells was partially rescued when NPM1, but not MYBBP1A, was knocked down (Fig. 4C). However, the enhanced transcriptional activities of p53 in SNORD17-knockdown cells were inhibited when MYBBP1A was impaired (Supplementary Fig. S7D). These results suggest that NPM1 may be involved regulating p53 expression by SNORD17, and MYBBP1A may be involved the regulation of p53 activity by SNORD17.

Neither knockdown nor overexpression of SNORD17 altered the mRNA levels of p53 (Supplementary Fig. S8A). However, increased SNORD17 reduced the half-life of p53 protein in HCC cells treated with CHX and vice versa (Fig. 4D; Supplementary Fig. S8B). Treatment of cells with MG132 diminished the effects of SNORD17 on the p53 protein levels, indicating that SNORD17 promoted p53 proteasomal degradation (Fig. 4E; Supplementary Fig. 8C).

Knockout or knockdown of SNORD17 decreased the poly-ubiquitination of p53, while the opposite effects were observed in SNORD17-overexpressing cells (Fig. 4F; Supplementary Fig. S8D). MDM2 is a well-recognized E3 ubiquitin ligase that regulates p53 stability, which could be disrupted by NPM1 [30, 32, 33]. Thus, we speculated that SNORD17 might regulate the protein level of p53 *via* MDM2. Knockdown of MDM2 diminished the effects of SNORD17 on levels of p53 protein and ubiquitination (Fig. 4G; Supplementary Fig. S8E). Collectively, these results indicate that SNORD17 promotes the MDM2-mediated degradation of p53 *via* NPM1.

SNORD17 promotes p300-mediated p53 acetylation *via* MYBBP1A

As the previous results, MYBBP1A-mediated SNORD17 activated p53 transcription instead of regulation on p53 expression. Acetylation modification is crucial for the activation of p53 [34, 35], and MYBBP1A was reported to enhance p53

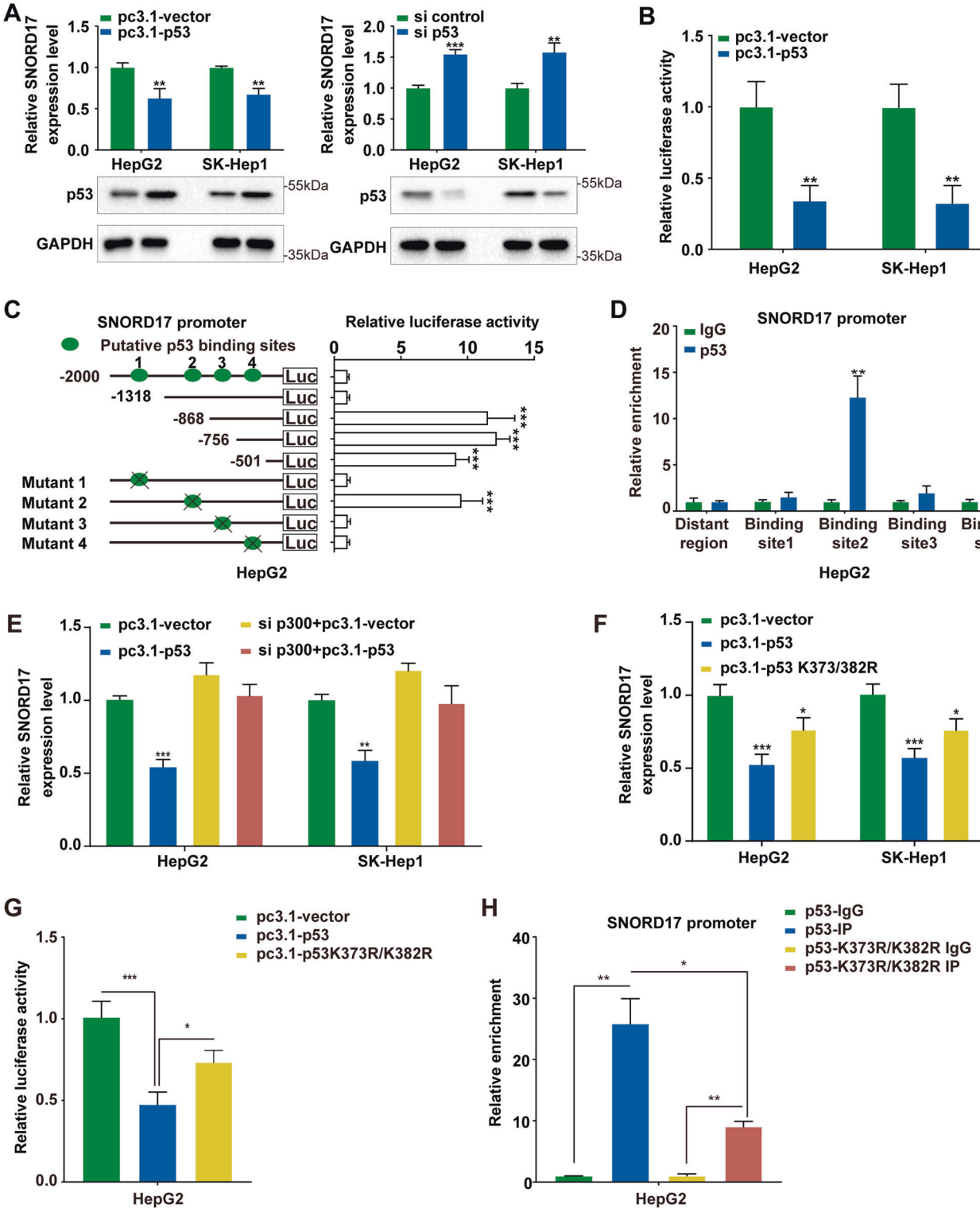

Fig. 7 p53 represses SNORD17 expression *via* a p300-dependent manner. A The expression levels of SNORD17 were detected by qRT-PCR in HepG2 and SK-Hep1 cells transfected with pcDNA3.1-p53 plasmids (pc3.1-p53) or p53 siRNA. **B** The promoter activity of SNORD17 was determined by dual-luciferase assay in cells transfected with pcDNA3.1-p53 plasmids. **C** Schematic diagram of the 4 putative p53-binding sites located in the promoter region of SNORD17 and the pGL4.17 based SNORD17 promoter reporter constructs (left). The transcriptional activity of the luciferase reporter constructs with WT and mutant p53-binding sites (site1: ACTTGTCCAAGTTAG; site2: ACATGTTTGGACAGA; site3: ACAGCTTGAGGCAAG; site4: CGTTGCACAGACGTG) were determined by dual-luciferase assay (right). **D** The binding between p53 and putative binding sites in SNORD17 promoter was determined by ChIP assay. **E** The expression of SNORD17 was measured by qRT-PCR in p53-overexpression HepG2 cells with or without transfection of p300 siRNA. **F** The expression of SNORD17 was measured by qRT-PCR in HepG2 and SK-Hep1 cells transfected with pcDNA3.1-p53 K373/382R mutant. **G** Dual-luciferase assay of SNORD17 promoter activity was carried out after transfecting pcDNA3.1-vector, pcDNA3.1-p53 or pcDNA3.1-p53 K373/382R plasmid in HepG2 cells. **H** qRT-PCR analysis of SNORD17 promoter abundance in ChIP assay for HepG2 cells transfecting pcDNA3.1-p53 or pcDNA3.1-p53 K373/382R plasmids. In (**A**–**H**), data are shown as mean ± SEM; $n = 3$ independent experiments. The statistical significance was determined by Student's two-tailed *t* test. $^{*}P < 0.05$; $^{**}P < 0.01$; $^{***}P < 0.001$. siRNA small interference RNA.

tetramerization and acetylation in response to nucleolar disruption in MCF-7 and H1299 cells [31]. Loss or knockdown of SNORD17 increased the acetylation levels of the p53 protein, whereas overexpression of SNORD17 decreased the acetylation of p53 at the K373 and K382 residues (Fig. 5A1, A2; Supplementary Fig. S9A). Moreover, the increase in p53 acetylation in SNORD17-KO cells was inhibited when MYBBP1A was knocked down (Fig. 5B1, B2), indicating MYBBP1A was indispensable for SNORD17 mediated p53 acetylation. To identify the acetyltransferases or deacetylases that are responsible for SNORD17/MYBBP1A regulated acetylation of p53, we screened four well-known acetyltransferases and deacetylases that could mediate the p53 acetylation at lysine 373/382 using specific siRNA. We identified that the knockdown of p300 blocked the increase of p53 acetylation in SNORD17-KO cells (Fig. 5C1, C2; Supplementary Fig. S9B). Co-IP assay confirmed that endogenous MYBBP1A binds p53 and p300 (Fig. 5D). We next explored the effects of MYBBP1A on the interaction between p53 and p300. Co-IP assays showed that overexpression of MYBBP1A in HepG2 cells significantly enhanced the association of p53 with p300 (Fig. 5E). Collectively, these results suggest that SNORD17 promotes p300-mediated p53 acetylation *via* MYBBP1A.

SNORD17 anchors NPM1 and MYBBP1A in the nucleolus

To further investigate how SNORD17 influences the stability and activity of p53 *via* NPM1 and MYBBP1A, respectively, we evaluated the impacts of SNORD17 on NPM1 and MYBBP1A. Western blot showed that altering the levels of SNORD17 did not affect the expression levels of NPM1 and MYBBP1A (Supplementary Fig. S10A). At the same time, subcellular fractionation and IF assays demonstrated that knockout of SNORD17 promoted the translocation of MYBBP1A and NPM1 from the nucleolus to the nucleoplasm (Fig. 6A; Supplementary Fig. S10B). Co-IP experiments showed that knockout of SNORD17 increased the binding between MDM2 and NPM1, as well as that between MYBBP1A, p53, and p300 (Fig. 6B, C). Significantly, reintroduction of SNORD17 in SNORD17-KO cells rescued the translocation of MYBBP1A and NPM1 from the nucleolus into the nucleoplasm, while also inhibited the interaction between NPM1 and MDM2, as well as p53, p300 and MYBBP1A (Supplementary Fig. S10C–E). Taken together, these data demonstrate that SNORD17 simultaneously binds NPM1 and MYBBP1A, and anchors them in the nucleolus, which inhibits the formation of NPM1-MDM2 and MYBBP1A-p53 complexes in the nucleoplasm.

Furthermore, endogenous co-IP showed NPM1 binds MYBBP1A, while IF showed the colocalization of MYBBP1A and NPM1 in the nucleolus (Fig. 6D; Supplementary Fig. S10F). We were intrigued by these findings implicating RNAs in protein-protein interaction and thus hypothesized that the interaction between NPM1 and the MYBBP1A might also involve SNORD17. Co-IP experiments exhibited that the binding between NPM1 and MYBBP1A was not affected by DNase, but this interaction was disrupted by RNase A (Fig. 6D). Moreover, co-IP experiments showed that depletion of SNORD17 largely abrogated the interaction between NPM1 and MYBBP1A (Fig. 6E). A series of NPM1 and MYBBP1A truncations carrying a nucleolar localization sequence (NoLS) (Fig. 6F1) was generated to identify the binding regions of MYBBP1A or NPM1 with SNORD17. RIP assays exhibited that MYBBP1A truncations containing the C-terminal domain and NPM1 truncations containing nucleotide-binding domain (NBD) interacts with SNORD17 (Fig. 6F2, F3).

p53 represses SNORD17 expression *via* a p300-dependent positive feedback loop

p53 is widely known for its role as a transcription factor, which prompted us to explore the impact of p53 in SNORD17 expression [36, 37]. Ectopic expression of p53 reduced SNORD17 expression, whereas knockdown of p53 increased SNORD17 expression (Fig. 7A). Luciferase reporter assays illustrated that p53 expression decreased the transcriptional activity of SNORD17 (Fig. 7B). We identified four putative p53-binding sites within the promoter region of SNORD17 using bioinformatics databases (JASPAR CORE). Mutation experiments indicated that the second p53-binding site (Bs2) was essential for reducing promoter activity by p53 (Fig. 7C). ChIP assays confirmed that the Bs2 sequence co-precipitated with endogenous p53 (Fig. 7D). Given the functions mentioned above of SNORD17 on p300-mediated p53 acetylation, we were curious whether p300-mediated p53 acetylation affects the SNORD17 expression. The reduction of SNORD17 expression induced by p53 was abolished when p300 was knocked down (Fig. 7E). Also, the inhibition of the transcriptional activity of SNORD17 and the binding of p53 on SNORD17 promoter was partially attenuated when transfected with the p53-mutant (p53 K373/382R) plasmids compared with p53 WT plasmids (Fig. 7F–H). Collectively, these data support the transcription inhibition of SNORD17 by p53 *via* p300-mediated acetylation, acting through a positive feedback mechanism.

Clinical significance of SNORD17 in HCC patients with wild-type p53

We further verified the correlation between SNORD17 and p53 signaling in HCC patients. There were negative correlations between the expression of SNORD17 and protein levels of p53, $p21^{CIP1}$ or Puma in clinical samples of HCC (Fig. 8A). Since p53 is frequently mutated in HCC, we determined the p53 mutations in cohort 3 and divided them into two groups: p53 wild-type and p53-mutated [16]. Kaplan–Meier analysis showed that higher SNORD17 expression was correlated with shorter OS and RFS in patients with wide-type p53, whereas this correlation was not observed in p53-mutated HCC cases (Fig. 8B).

SNORD17 is a promising target for the HCC therapy

To verify the validity of SNORD17 as a potential antitumor target in vivo, mice bearing HepG2 cells were treated with SNORD17 ASO or control ASO. The SNORD17 ASO succeeded to inhibit the growth of the subcutaneous and orthotopic tumors (Fig. 8C, D,

Supplementary Fig. S11A–E). In addition, decreased expression of SNORD17 and increased p53 protein levels were found in subcutaneous tumor tissues from the SNORD17 ASO treated mice (Supplementary Fig. S11C, F). These results suggest that SNORD17 is a promising target for HCC therapy.

DISCUSSION

Data are accruing about the associations between snoRNAs and oncogenesis or cancer progression [10], but the precise mechanism of their function in cell transformation is mainly unknown. Based on the well-characterized biology of canonical snoRNAs in

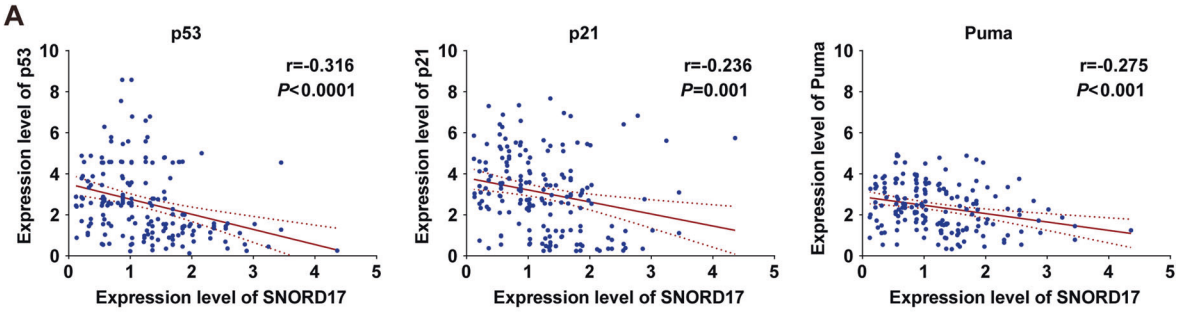

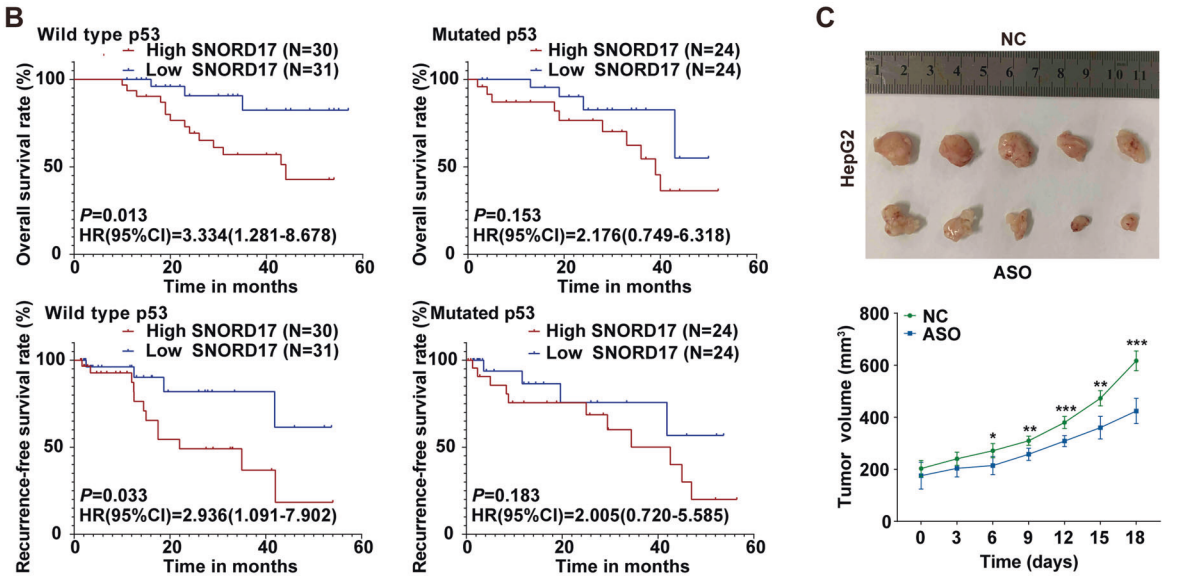

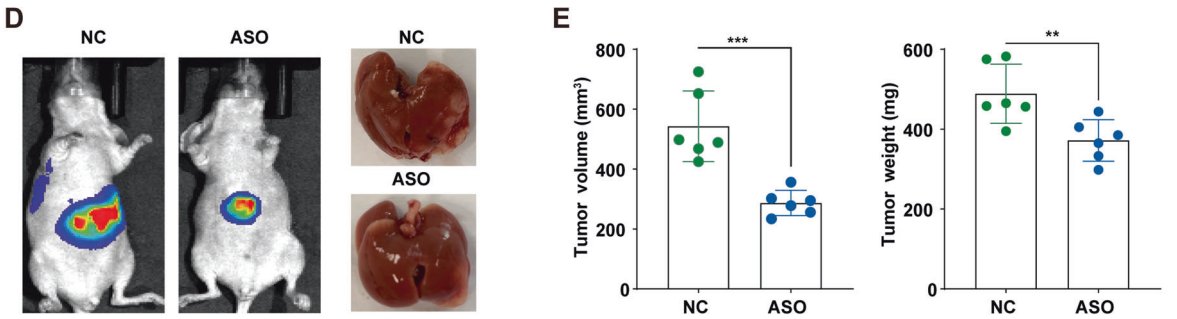

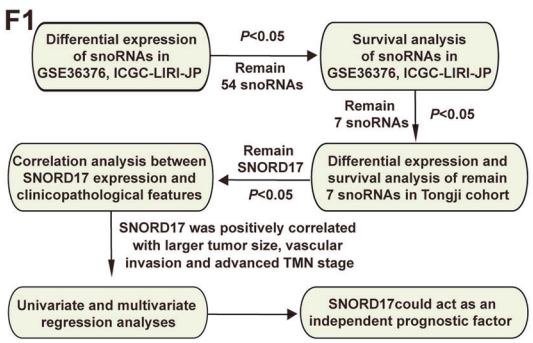

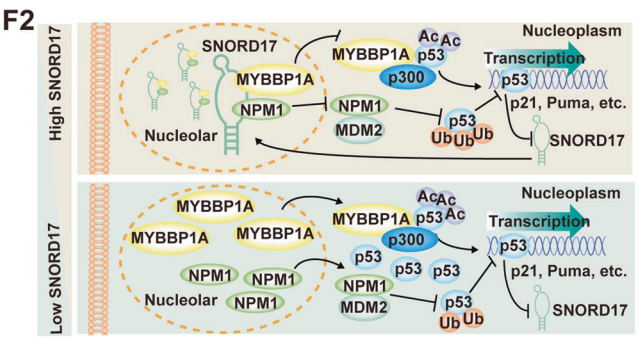

Fig. 8 Clinical significance of SNORD17 in HCC patients with wild-type p53 and the therapeutical application of SNORD17. A Analyses for the expression correlations between SNORD17 and the protein levels of p53, p21, and Puma in HCC cohort 3. **B** Kaplan–Meier analysis of the correlation between SNORD17 expression and OS or RFS of patients in the HCC cohort 3 with different genomic p53 mutation status. **C** Macroscopic images (upper) and growth curves (lower) of subcutaneous tumors from nude mice treated with intra-tumoral injection of SNORD17 ASOs (ASO) or negative control ASOs (NC) ($n = 5$ mice/group). **D** Representative bioluminescence and macroscopic images of orthotopic tumor from nude mice treated with intraperitoneal injections of SNORD17 ASOs (ASO) or negative control ASOs (NC) ($n = 6$ mice/group). **E** Quantification analysis of tumor volume and tumor weight in (**D**). (**F1**) Graphical summary of the flow chart analysis of HCC-related snoRNAs. (**F2**) Graphical summary of the molecular mechanisms of SNORD17, MYBBP1A, NPM1, and P53 in the regulation of tumor progression in HCC. In (**C**, **E**), data are represented as mean ± SEM. The statistical significance was determined by spearman rank correlation analysis (**A**), log-rank test (**B**), and Student's two-tailed *t* test (**C**, **E**). HR hazard rate, 95% CI 95% confidence intervals, NC negative control ASOs, ASO anti-SNORD17 ASOs.

ribosome biogenesis, their role in tumorigenesis was mainly focused on impaired ribosome production and the resulting translational deficiencies. However, a growing number of snoRNAs have been identified in recent studies to exhibit their noncanonical functions relevant to tumorigenesis. For example, SNORD50A and SNORD50B directly binds K-Ras, and inhibits K-Ras and Ras-ERK1/ERK2 signaling in human cancer [38]. SnoRNAs also serve as substrates for processing into smaller, microRNA-like species and the target pre-mRNAs in ways that impact alternative splicing, mRNA translation repression, and mRNA turnover [39–41]. As for SNORD17, a C/D box snoRNAs, could assemble proteins to form canonical snoRNPs and guide 2′-O-ribose methylation of rRNA [15]. Our results demonstrate that it is a novel promoter of and prognostic marker for HCC. SNORD17 interacts with NPM1 and MYBBP1A and inhibits their translocation to the nucleoplasm leading to an inhibition of p53 signaling (Fig. 8F1, F2). As has been reported, we have found two novel snoRNA binding proteins that do not belong to canonical snoRNPs. However, the results in this article cannot bear out whether the interaction of SNORD17 with NPM1 and MYBBP1A depends on canonical snoRNPs. More snoRNA binding proteins and functions of these snoRNA binding proteins deserve further discovery to reveal the function of snoRNA in pathophysiological processes.

The p53 protein acts as a tumor suppressor by regulating various cellular events, including cell cycle arrest and apoptosis, following signals such as oncogenic transformation or DNA damage [20, 36]. Therefore, it is of great importance to explore the regulatory mechanisms upstream and downstream of p53. Previous studies have shown that the expression and transcriptional activity of p53 are tightly regulated at multiple levels. NPM1 is a highly abundant protein that mainly resides in nucleoli and involves in multiple cellular functions including ribosome biogenesis and chromatin remodel [42]. Previous reports found that several proteins bind NPM1 and disrupt the interaction of NPM1 and MDM2 leading to a stabilization of p53 [43, 44]. Although NPM1 is a bona fide RNA-binding protein, little is known about its regulation by RNA [45]. Here, we found that SNORD17 binds NPM1 and impede its translocation to the nucleoplasm, which promote the association between p53 and MDM2. On the other hand, the acetylation of p53 can enhance its sequence-specific DNA binding and recruitment of a coactivator complex to the promoter regions to activate p53 target gene expression. However, there are few reports on the involvement of ncRNAs in the acetylation of p53. A prior study showed that MYBBP1A promotes p300-mediated p53 acetylation under nucleolar stress [31]. Herein, we found that SNORD17 suppresses the p300-regulated acetylation of p53 by binding to MYBBP1A and inhibiting its translocation into the nucleoplasm. These results demonstrate that SNORD17 modulates p53 stability and activity in HCC and add a new level of complexity in the regulation of p53 network.

DATA AVAILABILITY

All datasets on which the conclusions of the paper rely are attached in the main paper or additional supporting files.

REFERENCES

1. Siegel RL, Miller KD, Jemal A. Cancer statistics, 2020. CA Cancer J Clin. 2020;70:7–30.
2. Villanueva A. Hepatocellular carcinoma. N Engl J Med. 2019;380:1450–62.
3. El-Serag HB. Hepatocellular carcinoma. N Engl J Med. 2011;365:1118–27.
4. Sung H, Ferlay J, Siegel RL, Laversanne M, Soerjomataram I, Jemal A, et al. Global cancer statistics 2020: GLOBOCAN estimates of incidence and mortality worldwide for 36 cancers in 185 countries. CA Cancer J Clin. 2021;71:209–49.
5. Lafontaine DL, Tollervey D. Birth of the snoRNPs: the evolution of the modification-guide snoRNAs. Trends Biochem Sci. 1998;23:383–8.
6. Weinstein LB, Steitz JA. Guided tours: from precursor snoRNA to functional snoRNP. Curr Opin Cell Biol. 1999;11:378–84.
7. Tollervey D, Kiss T. Function and synthesis of small nucleolar RNAs. Curr Opin Cell Biol. 1997;9:337–42.
8. Cui L, Nakano K, Obchoei S, Setoguchi K, Matsumoto M, Yamamoto T, et al. Small nucleolar noncoding RNA SNORA23, up-regulated in human pancreatic ductal adenocarcinoma, regulates expression of spectrin repeat-containing nuclear envelope 2 to promote growth and metastasis of xenograft tumors in mice. Gastroenterology. 2017;153:292–306.e2.
9. Okugawa Y, Toiyama Y, Toden S, Mitoma H, Nagasaka T, Tanaka K, et al. Clinical significance of SNORA42 as an oncogene and a prognostic biomarker in colorectal cancer. Gut. 2017;66:107–17.
10. Liang J, Wen J, Huang Z, Chen XP, Zhang BX, Chu L. Small nucleolar RNAs: insight into their function in cancer. Front Oncol. 2019;9:587.
11. Donsante A, Miller DG, Li Y, Vogler C, Brunt EM, Russell DW, et al. AAV vector integration sites in mouse hepatocellular carcinoma. Science. 2007;317:477.
12. Pauli C, Liu Y, Rohde C, Cui C, Fijalkowska D, Gerloff D, et al. Site-specific methylation of 18S ribosomal RNA by SNORD42A is required for acute myeloid leukemia cell proliferation. Blood. 2020;135:2059–70.
13. Wang PR, Xu M, Toffanin S, Li Y, Llovet JM, Russell DW. Induction of hepatocellular carcinoma by in vivo gene targeting. Proc Natl Acad Sci USA. 2012;109:11264–9.
14. Xu G, Yang F, Ding CL, Zhao LJ, Ren H, Zhao P, et al. Small nucleolar RNA 113-1 suppresses tumorigenesis in hepatocellular carcinoma. Mol Cancer. 2014;13:216.
15. Huttenhofer A, Kiefmann M, Meier-Ewert S, O'Brien J, Lehrach H, Bachellerie JP, et al. RNomics: an experimental approach that identifies 201 candidates for novel, small, non-messenger RNAs in mouse. EMBO J. 2001;20:2943–53.
16. Levine AJ. p53, the cellular gatekeeper for growth and division. Cell. 1997;88:323–31.
17. Farmer G, Bargonetti J, Zhu H, Friedman P, Prywes R, Prives C. Wild-type p53 activates transcription in vitro. Nature. 1992;358:83–6.
18. Reed SM, Quelle DE. p53 acetylation: regulation and consequences. Cancers. 2014;7:30–69.
19. Levine AJ, Oren M. The first 30 years of p53: growing ever more complex. Nat Rev Cancer. 2009;9:749–58.
20. Whibley C, Pharoah PD, Hollstein M. p53 polymorphisms: cancer implications. Nat Rev Cancer. 2009;9:95–107.
21. Huang Z, Chu L, Liang J, Tan X, Wang Y, Wen J, et al. H19 promotes HCC bone metastasis through reducing OPG expression in a PPP1CA/p38MAPK-dependent manner and sponging miR-200b-3p. Hepatology. 2021;74:214–32.
22. Consortium EP. An integrated encyclopedia of DNA elements in the human genome. Nature. 2012;489:57–74.
23. Ernst J, Kheradpour P, Mikkelsen TS, Shoresh N, Ward LD, Epstein CB, et al. Mapping and analysis of chromatin state dynamics in nine human cell types. Nature. 2011;473:43–9.
24. Yu G, Wang LG, Han Y, He QY. clusterProfiler: an R package for comparing biological themes among gene clusters. Omics. 2012;16:284–7.
25. Subramanian A, Tamayo P, Mootha VK, Mukherjee S, Ebert BL, Gillette MA, et al. Gene set enrichment analysis: a knowledge-based approach for interpreting genome-wide expression profiles. Proc Natl Acad Sci USA. 2005;102:15545–50.
26. Falaleeva M, Pages A, Matuszek Z, Hidmi S, Agranat-Tamir L, Korotkov K, et al. Dual function of C/D box small nucleolar RNAs in rRNA modification and alternative pre-mRNA splicing. Proc Natl Acad Sci USA. 2016;113:E1625–34.

27. Hacot S, Coute Y, Belin S, Albaret MA, Mertani HC, Sanchez JC, et al. Isolation of nucleoli. Curr Protoc Cell Biol. 2010;Chapter 3:Unit3.36.
28. Barretina J, Caponigro G, Stransky N, Venkatesan K, Margolin AA, Kim S, et al. The cancer cell line encyclopedia enables predictive modelling of anticancer drug sensitivity. Nature. 2012;483:603–7.
29. Chuong EB, Elde NC, Feschotte C. Regulatory evolution of innate immunity through co-option of endogenous retroviruses. Science. 2016;351:1083–7.
30. Kurki S, Peltonen K, Latonen L, Kiviharju TM, Ojala PM, Meek D, et al. Nucleolar protein NPM interacts with HDM2 and protects tumor suppressor protein p53 from HDM2-mediated degradation. Cancer Cell. 2004;5:465–75.
31. Ono W, Hayashi Y, Yokoyama W, Kuroda T, Kishimoto H, Ito I, et al. The nucleolar protein Myb-binding protein 1A (MYBBP1A) enhances p53 tetramerization and acetylation in response to nucleolar disruption. J Biol Chem. 2014;289:4928–40.
32. Soussi T, Wiman KG. Shaping genetic alterations in human cancer: the p53 mutation paradigm. Cancer Cell. 2007;12:303–12.
33. Klein C, Vassilev LT. Targeting the p53-MDM2 interaction to treat cancer. Br J Cancer. 2004;91:1415–9.
34. Bode AM, Dong Z. Post-translational modification of p53 in tumorigenesis. Nat Rev Cancer. 2004;4:793–805.
35. Gu W, Roeder RG. Activation of p53 sequence-specific DNA binding by acetylation of the p53 C-terminal domain. Cell. 1997;90:595–606.
36. Levine AJ. p53: 800 million years of evolution and 40 years of discovery. Nat Rev Cancer. 2020;20:471–80.
37. Joerger AC, Fersht AR. The p53 pathway: origins, inactivation in cancer, and emerging therapeutic approaches. Annu Rev Biochem. 2016;85:375–404.
38. Siprashvili Z, Webster DE, Johnston D, Shenoy RM, Ungewickell AJ, Bhaduri A, et al. The noncoding RNAs SNORD50A and SNORD50B bind K-Ras and are recurrently deleted in human cancer. Nat Genet. 2016;48:53–8.
39. Kishore S, Khanna A, Zhang Z, Hui J, Balwierz PJ, Stefan M, et al. The snoRNA MBII-52 (SNORD 115) is processed into smaller RNAs and regulates alternative splicing. Hum Mol Genet. 2010;19:1153–64.
40. Ender C, Krek A, Friedlander MR, Beitzinger M, Weinmann L, Chen W, et al. A human snoRNA with microRNA-like functions. Mol Cell. 2008;32:519–28.
41. Brameier M, Herwig A, Reinhardt R, Walter L, Gruber J. Human box C/D snoRNAs with miRNA like functions: expanding the range of regulatory RNAs. Nucleic Acids Res. 2011;39:675–86.
42. Box JK, Paquet N, Adams MN, Boucher D, Bolderson E, O'Byrne KJ, et al. Nucleophosmin: from structure and function to disease development. BMC Mol Biol. 2016;17:19.
43. Fukawa T, Ono M, Matsuo T, Uehara H, Miki T, Nakamura Y, et al. DDX31 regulates the p53-HDM2 pathway and rRNA gene transcription through its interaction with NPM1 in renal cell carcinomas. Cancer Res. 2012;72:5867–77.
44. Wang J, Ding S, Duan Z, Xie Q, Zhang T, Zhang X, et al. Role of p14ARF-HDM2-p53 axis in SOX6-mediated tumor suppression. Oncogene. 2016;35:1692–702.
45. Castello A, Fischer B, Eichelbaum K, Horos R, Beckmann BM, Strein C, et al. Insights into RNA biology from an atlas of mammalian mRNA-binding proteins. Cell. 2012;149:1393–406.

ACKNOWLEDGEMENTS

We would like to thank Prof. Chaoyang Li (Affiliated Cancer Hospital and Institute of Guangzhou Medical University, State Key Laboratory of Respiratory Disease, Guangzhou, 510095, China.) for his kind suggestions on manuscript composition. We would like to thank Prof. Jiahuai Han (State Key Laboratory of Cellular Stress Biology, Innovation Center for Cell Signaling Network, Department of Biology, School of Life Sciences, Xiamen University, Xiamen, 361005, China.) for donating plasmids. We thank Shanghai Bioprofile Technology Company Ltd for technological assistance in mass spectrum assay. This study was supported by the National Natural Science Foundation of China (Nos. 82172971, 31671348, 81874065, 81874189), the National Key Research and Development Program of China (2018YFA0208904), Chen Xiaoping Foundation for the Development of Science and Technology of Hubei Province under Grant (CXPJJH12000001-2020317).

AUTHOR CONTRIBUTIONS

BXZ, XPC, LC, PKD, and JNL designed the experiments. JNL, GXL, ZH, and JYL performed most of the experiments and acquisition of data with assistance from ZH, JYW, WQX, ZYC, GZC, ZYD, HFL, and YW. JNL, ZH, PKD, and GXL wrote the paper and critically reviewed the paper. All authors read and approved the final version of the paper.

COMPETING INTERESTS

The authors declare no competing interests.

ETHICS APPROVAL

Animal experimental procedures were approved by the Committee on the Ethics of Animal Experiments of Tongji Hospital (TJH-201809003). Use of tissue from HCC patients was approved by the Ethics Committee of Tongji Hospital, Tongji Medical College, Huazhong University of Science and Technology (Wuhan, China) (TJ-IRB20210924).

ADDITIONAL INFORMATION

Supplementary information The online version contains supplementary material available at https://doi.org/10.1038/s41418-022-00929-w.

Correspondence and requests for materials should be addressed to Liang Chu, Xiaoping Chen or Bixiang Zhang.

Reprints and permission information is available at http://www.nature.com/reprints

Publisher's note Springer Nature remains neutral with regard to jurisdictional claims in published maps and institutional affiliations.

View publication stats